HHS Public Access

Author manuscript

Eur J Pharm Sci. Author manuscript; available in PMC 2020 October 01.

Published in final edited form as:

Eur J Pharm Sci. 2019 October 01; 138: 105032. doi:10.1016/j.ejps.2019.105032.

A systems pharmacokinetic/pharmacodynamic model for concizumab to explore the potential of anti-TFPI recycling antibodies

Dongfen Yuan[a], **Frederik Rode**[b], **Yanguang Cao**[a,c,*]

[a]Division of Pharmacotherapy and Experimental Therapeutics, UNC Eshelman School of Pharmacy, University of North Carolina at Chapel Hill, Chapel Hill, North Carolina 27599, USA;

[b]Novo Nordisk, Denmark; Translational DMPK, H. Lundbeck A/S;

[c]Lineberger Comprehensive Cancer Center, University of North Carolina at Chapel Hill, Chapel Hill, North Carolina 27599, USA.

Abstract

Concizumab is a humanized monoclonal antibody in clinical investigation directed against membrane-bound and soluble tissue factor pathway inhibitor (mTFPI and sTFPI) for treatment of hemophilia. Concizumab displays a non-linear pharmacokinetic (PK) profile due to mTFPI-mediated endocytosis and necessitates a high dose and frequent dosing to suppress the abundant sTFPI, a negative regulator of coagulation. Recycling antibodies that can dissociate bound mTFPI/sTFPI in endosomes for degradation and rescue antibody from degradation have a potential in reducing the dose by extending antibody systemic persistence and sTFPI suppression. We developed a systems PK/pharmacodynamics (PD) model with nested endosome compartments to simulate the effect of decreased antibody binding to mTFPI/sTFPI in endosomes on antibody clearance and sTFPI suppression for exploring the potential of anti-TFPI recycling antibodies in reducing the dose. A dynamic model-building strategy was taken. A reduced PK/PD model without the endosome compartments was developed to optimize unknown target turnover parameters using concizumab PK data. The optimized parameters were then employed in the systems PK/PD model for simulations. The obtained systems PK/PD model adequately described the PK of concizumab in rabbits, monkeys, and humans and the PD in humans. The systems PK/PD model predicted that an anti-TFPI recycling antibody with a 100-fold higher mTFPI/sTFPI dissociation constant in endosomes than concizumab can extend sTFPI suppression from 12 days to 1 month. Thus, the systems PK/PD model provides a quantitative platform for guiding the engineering and translational development of anti-TFPI recycling antibodies.

[*]Corresponding author: Yanguang Cao, UNC Eshelman School of Pharmacy, UNC at Chapel Hill., Address: 2318 Kerr Hall, 301 Pharmacy Lane, Chapel Hill, NC, 27599, Tel: (919) 966-4040, yanguang@unc.edu.

6. Declarations of interest

F. Rode was an employee of Novo Nordisk, Denmark and is an employee of H. Lundbeck A/S. Concizumab is an investigational drug of Novo Nordisk.

Graphical Abstract

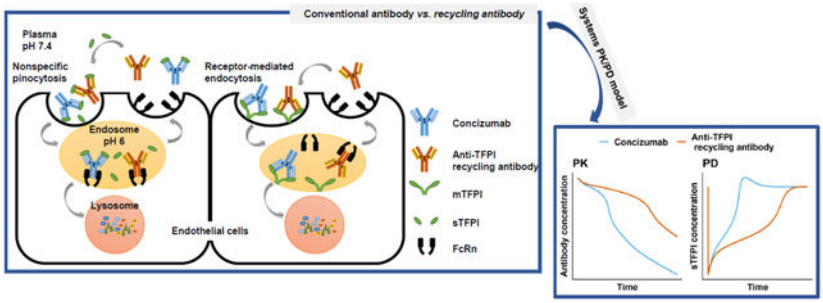

Keywords

Concizumab; target-mediated drug disposition; tissue factor pathway inhibitor; recycling antibody; FcRn; pharmacokinetics modeling

1. Introduction

Immunoglobulin G (IgG) has gained popularity as therapeutic agents owing to its long circulation half-life and high binding specificity to the targets (Dostalek et al., 2013). The long circulation half-lives of IgG-based therapeutic antibodies primarily relate to recycling mediated by the neonatal Fc receptor (FcRn), which is mainly expressed in the endothelial cells (Kuo and Aveson, 2011; Latvala et al., 2017). Serum proteins and antibodies are constantly internalized into endothelial cells *via* nonspecific pinocytosis and subsequently sorted to acidic endosomes. In the acidic endosomes, the IgGs that can bind to the FcRn *via* their Fc domain are recycled by FcRn to the cell surface whereas the serum proteins and immunoglobulins that cannot bind to the FcRn are sorted to lysosomes for degradation (Roopenian and Akilesh, 2007). At the cell surface where the pH increases to neutral, antibodies bound to FcRn are released back to the plasma (Roopenian and Akilesh, 2007). Thus, IgGs (IgG_1. IgG_2, and IgG_4) exhibit long circulation half-lives (roughly 18–21 days in humans) (Ryman and Meibohm, 2017). The catabolism in lysosomes is a clearance pathway shared by all antibodies.

Most antibodies with the Fab domain bound to the soluble targets can still be recycled by FcRn, displaying similar slow antibody clearance as free antibody. But the bound soluble targets can be rescued by FcRn from lysosomal degradation along with the antibodies (Igawa et al., 2014). In addition, the antibodies remain occupied by the tightly bound targets during their entire lifetime. Although these antibodies have long circulation, they have only one chance of neutralizing the soluble targets (Igawa et al., 2014). Antibodies bound to transmembrane targets are internalized into cells *via* receptor-mediated endocytosis (Igawa et al., 2014; Mager, 2006; Wang et al., 2012). In the endosomes, the membrane targets-anchored antibodies cannot bind to FcRn and are sorted to lysosomes for degradation (Igawa et al., 2014), resulting in short lifespan and non-linear clearance that is known as target-mediated drug disposition (TMDD) or the “antigen sink effect” (Krippendorff et al., 2009; Mager, 2006; Wang et al., 2012). For conventional antibodies that cannot dissociate the targets in endosomes, one molecule of soluble or membrane-bound target requires one

molecule of antibody. To overcome the “antigen sink effect” and compensate for the limited chance of target neutralization, a high dose and frequent dosing are required for conventional antibodies targeting soluble and membrane targets with fast turnover and high abundance.

Recycling antibodies have been developed to neutralize the targets at lower dose and dosing frequency in comparison to conventional antibodies (Igawa et al., 2010; Igawa et al., 2014; Sampei et al., 2018). Recycling antibodies display reduced target binding at the acidic pH and low calcium concentration found in endosomes (Hironiwa et al., 2016; Igawa et al., 2014). As shown in the graphical abstract in supplementary materials, recycling antibodies can release the soluble targets in the endosomes, allowing the antibodies to be recycled in the free form and to participate in another round of target neutralization (Igawa et al., 2014). By dissociating from the transmembrane targets in the endosomes, recycling antibodies can be recycled by FcRn and participate in another round of target binding (Igawa et al., 2014). Therefore, in comparison to conventional antibodies, recycling antibodies can recycle the antibodies for multiple rounds of target neutralization, reducing the dose and dosing frequency required for target blocking.

Concizumab is a humanized monoclonal IgG_4 that is currently under clinical evaluation for hemophilia treatment. It neutralizes tissue factor pathway inhibitor (TFPI), a negative regulator in the coagulation pathway, and reduces bleeding events in hemophilia patients (Peterson et al., 2016). It is known that TFPI exists in different isoforms, namely TFPI-α, TFPI-β, and truncated TFPI-α (Hansen et al., 2014). These TFPI isoforms distribute in three pools: one pool is associated with endothelial cells (~ 85%), including TFPI-α associated with cell surface glycosaminoglycan, TFPI-α and TFPI-β anchored on cell surface by glycosylphosphatidylinositol (GPI) co-receptor, and intracellular TFPI-α; the second pool circulates in the plasma (~ 10%), including full-length TFPI-α, truncated TFPI-α, and lipoprotein-bound TFPI-α; and the third pool is TFPI-α residing in the platelet (5%) (Broze and Girard, 2012; Gu et al., 2017; Hansen et al., 2014). Concizumab binds to the conserved Kunitz-type protease inhibitor 2 (K2) domain in all isoforms (Hansen et al., 2014). Concizumab can readily access the TFPI on the surface of endothelial cells (mTFPI) and the free TFPI circulating in the plasma (sTFPI). While both sTFPI and the TFPI in circulating platelets can migrate to the sites of vessel injury and inhibit coagulation (Parng et al., 2018), sTFPI is used as an exploratory pharmacodynamics (PD) marker for assessing hemophilia treatment due to its ease of sampling (Chowdary et al., 2015; Eichler et al., 2018; Peterson et al., 2016).

As concizumab is a conventional antibody that cannot dissociate sTFPI and mTFPI in endosomes. it requires high dose and frequent dosing to compensate for mTFPI-mediated antibody clearance and suppress sTFPI for treating hemophilia. In rabbits, monkeys, and humans, concizumab has shown nonlinear clearance faster clearance at low doses and slower clearance at high doses (Agerso et al., 2014; Chowdary et al., 2015; Hansen et al., 2014). The dose-dependent clearance is due to the limited mTFPI-mediated endocytosis. At high doses when all the mTFPI binding sites have been saturated by some concizumab, the remaining concizumab is cleared by only the non-specific pinocytosis, whereas at the low doses, concizumab is cleared by both the non-specific pinocytosis and the mTFPI-mediated endocytosis. A high dose and frequent dosing are therefore required for concizumab to

saturate newly-synthesized mTFPI and to maintain a high plasma concentration of antibody for neutralizing the negative coagulation factor, sTFPI. In a phase I clinical trial, concizumab at a dose as high as 9 mg/kg could only suppress sTFPI for 2 weeks (Chowdary et al., 2015). Two ongoing clinical trials of concizumab apply a daily dosing regimen (clinicaltrials.gov, and), which is far more frequent than the weekly or even monthly dosing regimens for typical therapeutic antibodies. Thus, strategies that can reduce the dose and dosing frequency are needed to reduce the cost and improve the comfort for hemophilia patients. Anti-TFPI recycling antibodies are currently under preclinical investigation as a strategy to improve the dosing regimen for hemophilia treatments.

Here, we propose a systems pharmacokinetics (PK)/PD model that can describe the PK and PD of concizumab, namely the mTFPI-driven non-linear clearance and the suppression of sTFPI, and can simulate the antibody-target dissociation in endosomes, to explore the potential of anti-TFPI recycling antibodies in improving the dosing regimen. The systems PK/PD model extends our prior general model structure for recycling antibodies targeting only soluble targets (Yuan et al., 2018) with a second endothelial endosome compartment for describing the membrane target-mediated antibody clearance. Due to the model complexity, we took a dynamic modeling strategy. We designed a reduced PK/PD model to optimize the unknown turnover parameters for mTFPI using the PK and PD data of concizumab in humans. The reduced model removes the endosome compartments and describes the target binding and the linear and non-linear clearance of antibody in the plasma compartment of a second-generation minimal physiologically-based PK (mPBPK) model (Cao et al., 2013). By integrating the optimized target turnover parameters from the reduced model, the systems PK/PD model was able to describe concizumab PK and PD in humans. Using this systems PK/PD model, we simulated the PK/PD of anti-TFPI recycling antibodies in humans and predicted the magnitude of affinity engineering required to improve the dosing regimen. The same systems PK/PD model was also able to describe concizumab PK in two preclinical animals, monkeys and rabbits, using species-dependent parameters. Thus, the systems PK/PD model provides a quantitative platform that can guide the translational development of anti-TFPI recycling antibodies.

2. Methods

2.1. Data sources

PK/PD data from the following sources were digitized using WebPlot Digitizer (https://automeris.io/WebPlotDigitizer): concizumab in humans (Chowdary et al., 2015), concizumab in monkeys (Agerso et al., 2014), concizumab and its Hz isotype control antibody in rabbits (Hansen et al., 2014), and bevacizumab and its Fc variant, Xtend in monkeys (Zalevsky et al., 2010). Molar concentrations were calculated using a molecular weight of 150 kDa for antibodies and 34 kDa for sTFPI (Parng et al., 2018).

2.2. The systems PK/PD model

TFPI-binding antibodies like concizumab are subject to linear and non-linear clearances. In the linear pathway, free antibody and the sTFPI-bound antibody are cleared from the plasma *via* nonspecific pinocytosis by the endothelial cells followed by catabolism in lysosomes or

recycling by FcRn. Due to the large capacity of lysosomal catabolism and FcRn recycling. this pathway is linear in the typical dose range of therapeutic antibodies except for intravenous IgG (IVIG. 200–400 mg/kg) (Jolles et al.. 2005; Roopenian and Akilesh. 2007). In the non-linear pathway, mTFPI-bound antibody is cleared *via* receptor-mediated endocytosis by the endothelial cells and subsequent catabolism in lysosomes.

To capture the two clearance pathways of TFPI-binding antibodies, a systems PK/PD model was developed by extending our prior general model for antibodies against soluble targets (Yuan et al., 2018). The prior general model nests an endothelial endosome compartment in the plasma compartment of a mPBPK model (Cao et al., 2013) to describe the linear clearance of free antibody and antibody-soluble target complex. This general model structure can be applied to describe the kinetics of free antibody and the sTFPI-bound antibody. The systems PK/PD model in this work extends the prior general model with a second endosome compartment for describing the membrane target pathway. The two endosome compartments (V_{e1} and V_{e2}) were nested in parallel with the plasma compartment (V_p) to represent the endothelial endosomes for the nonspecific pinocytosis and the receptor-mediated endocytosis. Model parameters are defined in Appendix I and described below. The model structure of the systems PK/PD model is shown in Figure 1 and defined by Appendix II Equation (1–23).

As shown in Figure 1, the free anti-TFPI antibody (A) binds to sTFPI and endothelial cell membrane-bound mTFPI in plasma. In the non-linear pathway, mTFPI-bound antibody (AmTFPI) is internalized into the endothelial endosome compartment (V_{e1}) by receptor-mediated endocytosis at a rate of k_{int}. In V_{e1}, the antibody dissociated from mTFPI (if any) can bind to FcRn and form the antibody-FcRn complex (FcRnA), which can be recycled to the plasma at a rate of k_{rec}; other proteins, including mTFPI, AmTFPI, and FcRn-unbound free antibody (A) are degraded at a clearance of CL_e. In the linear pathway, A, sTFPI, and antibody-sTFPI complex (AsTFPI) in plasma are internalized into endothelial endosome compartment (V_{e2}) by nonspecific pinocytosis at a clearance of CL_{up}. In V_{e2}, FcRn-bound A and AsTFPI (FcRnA and FcRnAsTFPI) are recycled back to plasma at k_{rec} and FcRn-unbound A, sTFPI and AsTFPI are degraded at CL_e. Consistent with the prior general model, we assumed that the A and AsTFPI bind to FcRn with equal binding affinity because the antibody binds to sTFPI and FcRn *via* different domains (Fab domain for sTFPI and Fc domain for FcRn).

Stable target turnover is assumed for each target as is typically assumed (Gibiansky and Gibiansky. 2009), meaning that the synthesis rate equals the product of the total degradation rate and target baseline (Appendix II Equation 3 and 5). mTFPI is synthesized at a zero order synthesis rate of k_{synm} and degraded at a first order degradation rate of k_{degm} by cell internalization. sTFPI is synthesized at a zero order synthesis rate of k_{syns} and cleared at a first order degradation rate of k_{degs} in total, which includes nonspecific pinocytosis by endothelial cells (CL_{up}) and other nonspecific pinocytosis-independent degradation pathways (k'_{degs}), such as enzymatic degradation in plasma. k'_{degs} was calculated by Appendix II Equation (3).

The tissue distribution of A and AsTFPI was described similarly as the prior general model (Yuan et al., 2018). The peripheral tissues are lumped into two groups based on tissue vascular structure and leakiness: the tight tissues with continuous vessels (V_1) and the leaky tissues with discontinuous vessels (V_2). A and AsTFPI follow the same peripheral disposition (Appendix II equation (18–23)): convection from plasma (V_p) to the peripheral tissues as defined by the lymph flows (L_1 and L_2) and vascular reflection coefficients (σ_1 and σ_2), recollection of tissue interstitial fluids into lymph (V_l) as defined by the lymph flows (L_1 and L_2) and lymphatic vascular reflection coefficient (σ_l), and recycling of lymph fluid (L) back to the plasma. The vascular reflection coefficients (σ_1, σ_2, and σ_l) reflect the level of resistance of blood and lymph vessels to the convective transport of antibodies: higher value represents more restricted convection (Rippe and Haraldsson, 1987).

For subcutaneous (SC) administration, an absorption depot compartment was introduced as described by Appendix II Equation (1). A model switcher with a value of zero for intravenous (IV) administration and 1 for SC administration was introduced in Appendix II Equation (2) to indicate the drug input mode.

2.3. Parameter optimization in the reduced PK/PD model

To improve parameter identifiability, a reduced PK/PD model without the endosome compartments was designed to optimize the unknown parameters: the mTFPI baseline ($mTFPI\_b$) and turnover rates (k_{int}, k_{degm}), using concizumab data in humans (Chowdary et al., 2015). In consistent with the systems PK/PD model, the reduced model used the mPBPK model as the base model and integrated target binding and antibody clearance in the plasma compartment. The model structure is shown in Figure S1. In the plasma compartment, because concizumab binds to the conserved K2 domain in sTFPI and mTFPI (Hansen et al., 2014), concizumab can bind to both targets with equal binding affinity and form the complexes (AsTFPI and AmTFPI). Because AmTFPI cannot be recycled by FcRn, AmTFPI is cleared from the system at k_{int}. AsTFPI can be recycled by FcRn similarly as free concizumab, thus AsTFPI is subject to the same linear clearance (CL_{linear}) as free concizumab. The plasma compartment of the reduced model is described by Appendix III Equation (24–28). The peripheral compartments stay the same as the systems PK/PD model (Appendix II Equations (18–23)).

Parameters for the mTFPI baseline and turnover rates were optimized in ADAPT 5, a computational modeling platform for PK and PD applications (D'Argenio et al., 2009), using the maximum likelihood method and a combined additive and proportional error model. The ADAPT 5 code is provided in the supplementary materials. The human PK data of total antibody and free sTFPI following IV injections of concizumab at doses of 0.25, 1, 3, and 9 mg/kg were used for parameter optimization (Chowdary et al., 2015). The mPBPK base model parameters were fixed to literature reports (Table 2). Several analysis strategies were tested and compared based on model evaluation criteria (Table S1 in supplementary materials). Note that the SC PK data were not included for parameter optimization and served as an external dataset to evaluate model performance. For that purpose, the bioavailability (F) and absorption rate constant (k_a) of concizumab in humans were fixed to reported values in monkeys (Agerso et al., 2014). Model evaluation criteria include visual

inspection, weighted residual plots, Akaike Information Criterion (AIC), Bayesian Information Criterion (BIC), and Coefficient of Variation (CV%) of the estimated parameters. Model diagnostic plots were plotted using an R package, ggplot2 (Ginestet, 2011).

2.4. Systems PK/PD model simulation of concizumab in humans

The mTFPI baseline (*mTFPI_b*), mTFPI turnover rate ($k_{int} = k_{degm}$), and the dissociation rate constant of concizumab-target complexes (AmTFPI and AsTFPI), k_{off}, optimized in the reduced model were applied to the systems PK/PD model for simulations. Because concizumab is not engineered to show pH/calcium-dependent target binding, the target binding kinetics in endosome (k_{eon} and k_{eoff}) were assumed the same as those in plasma (k_{on} and k_{off}). The parameters related to endosomal trafficking and FcRn recycling, such as nonspecific pinocytosis rate (CL_{up}), nonspecific catabolism rate (CL_e), and FcRn recycling rate (k_{rec}), were fixed to the values in our prior general model that were calibrated using a variety of antibodies (Yuan et al., 2018).

Model simulations were performed to predict PK of total antibody and sTFPI after IV or SC administration of concizumab at various doses in humans. The simulations were performed using an R package, RxODE (Wang et al., 2016). The R script for the systems PK/PD model in humans is provided in the supplementary materials. Model predictions were overlaid with observations to evaluate model performance using an R package, ggplot2 (Ginestet, 2011).

2.5. Explorations of anti-TFPI recycling antibodies in humans

Anti-TFPI recycling antibodies with altered target binding kinetics in endosomes were simulated based on the systems PK/PD model of concizumab by decreasing the antibody-target association rate constant (k_{eon}) or increasing the antibody-target dissociation rate constant (k_{eoff}) in the endosome compartments. These anti-TFPI recycling antibodies were assumed to have equal target binding kinetics in plasma (k_{on} and k_{off}) and FcRn binding kinetics (k_{1on} and k_{1off}) as concizumab. The model could also simulate other anti-TFPI recycling antibodies with different target binding kinetics in plasma and different FcRn binding kinetics.

2.6. Interspecies translation of the systems PK/PD model

The systems PK/PD model was also developed for monkeys and rabbits, two common preclinical species for hemophilia study, facilitating proof-of-concept experiments in preclinical animals before clinical studies. The interspecies translation was done by updating the systems PK/PD model with species-specific parameters. Species-specific physiological parameters, such as plasma volume (V_p), lymphatic flow (L), and sTFPI baseline (*sTFPI_b*), were fixed to literature reports (Table 2).

In the linear clearance pathway, CL_{up}, CL_e, antibody-FcRn binding kinetics (k_{1on} and k_{1off}), and FcRn concentration in endosomes (*FcRn b*) jointly define the linear clearance of antibodies (Yuan et al., 2018). It is impossible to identify all these parameters for monkeys and rabbits without fixing some of the parameters. Thus, some parameters were fixed to human values or scaled from human values based our current knowledge, and then the rest

were optimized. FcRn recycling rate (k_{rec}) was fixed to human value, which was calculated based on *in vitro* measurement of endosome trafficking time (Hopkins and Trowbridge, 1983; Yuan et al., 2018). The same endosome trafficking time was also used by others for mice (Chen and Balthasar, 2012). FcRn concentration in endosomes (*FcRn b*) was assumed the same across species as others assumed (Shah and Betts, 2012). The catabolism in lysosome (CL_e) was scaled across species based on body weight using a scaling factor of 0.75, which is commonly used to scale metabolism (Diao and Meibohm, 2015; Li et al., 2017). When not available in the literature, k_{1on} and k_{1off} were fixed to the values of adalimumab-human FcRn binding kinetics which was used to calibrate human CL_e in our prior general model (Yuan et al., 2018). Monkey FcRn and rabbit FcRn have been shown to bind human IgG at similar affinity as human FcRn (Szikora et al., 2017; Yeung et al., 2010). With the obtained k_{rec}, CL_e, *FcRn b*, k_{1on} *and* k_{1off}, the nonspecific pinocytosis rates (CL_{up}) in monkeys and rabbits were optimized. CL_{up} in monkeys and rabbits were selected to be optimized because scaled mice CL_{up} using a scaling exponent of 0.75 has been shown to be higher than the observed value (Yuan et al., 2018). The values of monkey and rabbit CL_{up} can later be validated by measuring the clearance of nonspecific antibodies in FcRn-knockout monkeys and rabbits when these animal models become available. The optimization was done in Berkeley Madonna v8.3.18 (Berkeley, CA) using the PK data of linearly cleared antibodies and our prior general model structure (Yuan et al., 2018). The Berkeley Madonna code is provided in supplementary materials. The PK data of bevacizumab and a bevacizumab's Fc-engineered variant, Xtend, and their reported monkey FcRn binding kinetics (Zalevsky et al., 2010) were used for model optimization of monkey CL_{up}. The PK data of a concizumab isotype control antibody (Hansen et al., 2014) were used to optimize rabbit CL_{up} with the unknown rabbit FcRn binding affinity assumed the same as adalimumab-human FcRn binding affinity. The isotype control matches concizumab on the FcRn-binding domain but lacks target specificity, thus it is a good candidate to calibrate the linear clearance pathway in rabbit for concizumab.

In the non-linear pathway, sTFPI/mTFPI turnover rates (k_{degs} and k_{degm}) were scaled from human values using a scaling exponent of −0.25 (Diao and Meibohm, 2015; Li et al., 2017). The mTFPI baselines for rabbits and monkeys were not reported. Because sTFPI and mTFPI are produced through alternative splicing of the same TFPI gene (Maroney et al., 2010), mTFPI baseline was assumed to be correlated with sTFPI baseline. Based on the levels of sTFPI baselines. mTFPI baselines in rabbits and monkeys were calculated from human mTFPI baseline based on the measurable sTFPI baseline as $human\ mTFPI\_b \times \frac{animal\ sTFPI\_b}{human\ sTFPI\_b}$. All monkey and rabbit parameters, their source, and calculations were summarized in Table 2.

2.7. Sensitivity analysis of the systems PK/PD model

Local sensitivity analysis was done by individually increasing or decreasing the parameter value 10-fold from the human value listed in Table 2. The ratio of area under the curve (AUC) of total concizumab and free sTFPI in 45 days after antibody administration was calculated as AUC_{after}/AUC_{before} where AUC_{before} and AUC_{after} are the AUCs before and

after parameter adjustment, respectively. The AUC was calculated using an R package, DescTools (al, 2018).

3. Results

3.1. Parameter optimization in the reduced PK/PD model

We developed a reduced PK/PD model to facilitate parameter optimization. The optimized parameters were then integrated into the systems PK/PD model for simulations. As shown in Figure S1 and described in section 2.3, the reduced PK/PD model describes the nonspecific linear clearance of free concizumab and sTFPI-bound concizumab (AsTFPI) and the non-linear clearance of mTFPI-bound concizumab (AmTFPI). The linear clearance was described by a single parameter, CL_{linear}, in the reduced model and by an endosome structure in the systems PK/PD model (Figure 1). We have previously validated the endosomal structure (CL_{up}, CL_e, and k_{rec}) for describing the nonspecific linear clearance of antibodies (Yuan et al., 2018). The same model structure and parameterization were used for concizumab in the systems PK/PD model as this linear pathway is common to all antibodies. To ensure proper integration of the parameters optimized in the reduced PK/PD model to the systems PK/PD model, CL_{linear} was fixed to the reported linear clearance of adalimumab (Cao and Jusko, 2014), the antibody that was used to calibrate the endosome kinetics (Yuan et al., 2018). While concizumab is a wild-type IgG_4 and adalimumab is a wild-type IgG_1, this assumption of similar linear clearance was supported by that the IgG isotype has a negligible influence on FcRn binding and that IgG_1 and IgG_4 have similar circulation half-life (Neuber et al., 2014; Vidarsson et al., 2014). The sTFPI baseline ($sTFPI\_b$) was fixed to 1.6 nM observed in humans (Chowdary et al., 2015). The total degradation rate of sTFPI (k_{degs}) was fixed to 1.18 day^{-1} measured in healthy volunteers in a clinical pulse-chase study (Farrokhi et al., 2018).

The unknown mTFPI baseline ($mTFPI\_b$) and turnover parameters (k_{degm}, k_{int}) were optimized in the reduced PK/PD model using the human PK data of total concizumab and free sTFPI after IV injections of the antibody at various doses. Several analysis plans have been evaluated: 1) fix concizumab-sTFPI/mTFPI association and dissociation rate constants (k_{on} and k_{off}) to *in vitro* measurements (Hilden et al., 2012); 2) optimize one or both of k_{on} and k_{off}; 3) assume or not assume mTFPI and AmTFPI have equal cell internalization rate ($k_{degm} = k_{int}$) as is typically assumed (Gibiansky and Gibiansky, 2010); 4) optimize or fix k_{degm}/k_{int} to *in vitro* measurement of the cell internalization rate of two membrane proteins (33.1 day^{-1}), the folate receptor and the decay accelerating factor, which are anchored by GPI similarly as TFPI-p, in monkey kidney epithelial (MA104) cells and Chinese hamster ovary (CHO) cells (Mayor et al., 1998). The final analysis plan was selected based on visual inspection, AIC, BIC, and CV% of estimated parameters (Table S1). The final selected model assumed $k_{degm} = k_{int}$, fixed k_{on} to *in vitro* measurement, and optimized k_{off}.

As shown in Table 1, most parameters were estimated with reasonable CV% (less than 30%) except for k_{off} (56%). However, fixing k_{off} to *in vitro* measurement resulted in poor model predictions of the sTFPI PK. The model estimate of mTFPI baseline was higher than the sTFPI baseline as expected (Broze and Girard, 2012; Gu et al., 2017; Hansen et al., 2014).

As shown in Figure S2, the optimized reduced PK/PD model adequately captured the PK of total concizumab in humans after IV injections of concizumab at multiple doses. The model captured the PK of sTFPI well at IV concizumab doses of 0.25 mg/kg and 1 mg/kg and fairly at 3 mg/kg, but failed to capture the earlier and slower recovery of sTFPI at 9 mg/kg. Manually adjusting antibody-mTFPI/sTFPI binding affinity did not improve model predictive performance for sTFPI. Nevertheless, as shown in Figure S3, most model predictions for total antibody and sTFPI concentrations were within two standard deviations of observations. The human PK data of total concizumab and sTFPI in humans after SC injections of concizumab at 1 mg/kg and 3 mg/kg were reserved as an external dataset for model validation. In Figure S2, using the SC bioavailability and absorption rate constant of concizumab reported for monkeys (Agerso et al., 2014), the reduced PK/PD model fairly captured the SC PK data of both antibody and sTFPI in humans. considering that the absorption of concizumab in humans has not been optimized yet. Note that due to the nonlinear clearance. the PK of concizumab would be greatly affected by absorption.

3.2. The systems PK/PD model simulations in humans

The optimized mTFPI parameters ($mTFPI\_b$ and k_{int}/k_{degm}) and concizumab-mTFPI/sTFPI dissociation rate constant (k_{off}) in the reduced PK/PD model were then integrated into the systems PK/PD model for simulations. For the simulation, we assumed that the antibody-target binding kinetics in the endosomes were the same as in the plasma ($k_{eon} = k_{on}$ and $k_{eoff} = k_{off}$) because concizumab is not engineered to release the antigens in endosomes. Using the previously calibrated endosome kinetics (CL_{up}, CL_e, and k_{rec}) for adalimumab (Yuan et al., 2018) and assuming that concizumab has similar FcRn binding kinetics as adalimumab as discussed above as explained in section 3.1, the systems PK/PD model adequately predicted the PK of total concizumab and sTFPI in humans after IV and SC administration (Figure 2).

3.3. Explorations of anti-TFPI recycling antibodies in humans

We simulated anti-TFPI recycling antibodies in humans by decreasing the antibody-mTFPI/sTFPI association rate constant (k_{eon}) or increasing the dissociation rate constant (k_{eoff}) in endosomes, while keeping the binding kinetics in plasma (k_{on} and k_{off}) unchanged. Figure 3 shows that a decrease in k_{eon} had minimal effects on the clearance of antibody and suppression of sTFPI, while an increase in k_{eoff} notably decreased antibody clearance and prolonged sTFPI suppression. At an equal dose of 3 mg/kg (one of clinically tested concizumab doses), anti-TFPI recycling antibodies with a 100-fold or higher target dissociation rate constant in endosomes (k_{eoff}) can suppress sTFPI below the lower limit of quantification (LLOQ) for 30 days or longer, compared to 12 days for concizumab (the black line). Further increasing the endosomal target dissociation rate constant beyond 1,000-fold had a smaller effect in prolonging antibody half-life and sTFPI suppression.

3.4. Interspecies translation of the systems PK/PD model

The goal of developing the systems PK/PD model is to provide a quantitative framework for facilitating the development of anti-TFPI recycling antibodies, including the preclinical studies in monkey and rabbits, two commonly used animal models for hemophilia study. Thus, we also parameterized the systems PK/PD model for these two species using species-

specific physiological parameters (such as V_p, L, and $sTFPI\_b$), allometrically scaled parameters (k_{degs}, k_{degm}/k_{int}, and CL_e), and individually optimized parameter (CL_{up}). Previously, we reported that the CL_{up} for mice estimated base on antibody clearance in FcRn knockout mice is lower than the allometrically scaled value from human CL_{up} using a scaling factor of 0.75 (Yuan et al., 2018). Thus, in Figure 4A and B, we optimized CL_{up} individually for monkeys and rabbits using the reported PK data of linearly cleared antibodies. The CL_{up} optimized for monkeys and rabbits in this work and the CL_{up} estimated for mice and humans (Yuan et al., 2018) were plotted against the logarithm of body weight. As shown in Figure 4C, the CL_{up} can be allometrically scaled across mice, monkeys, rabbits, and humans using a scaling exponent of 0.83 ($R^2 = 0.98$), which was in the range of scaling exponents reported for linearly cleared antibodies (0.69 – 0.83 (Oitate et al., 2011), 0.695 – 1.27 (Zhao et al., 2015), and 0.89 (Betts et al., 2018)).

Using the optimized CL_{up} for each species, we simulated concizumab in monkeys and rabbits. The association and dissociation rate constants of concizumab binding to sTFPI/mTFPI (k_{on} and k_{off}) and to FcRn ((k_{1on} and k_{1off})) in monkeys and rabbits were not available and thus were assumed the same as the values in humans. Monkey FcRn and rabbit FcRn have been shown to bind human IgG at very similar affinity as human FcRn (less than 3-fold difference in equilibrium dissociation constant) (Szikora et al., 2017; Yeung et al., 2010). sTFPI and mTFPI are produced through alternative splicing of the same TFPI gene (Maroney et al., 2010), thus the unknown mTFPI baselines in monkeys and rabbits were calculated based on the reported levels of sTFPI baselines (Table 2) The systems PK/PD model parameters for each species were listed in Table 2. Without further optimization, the systems PK/PD model adequately predicted the PK of concizumab in monkeys and rabbits under different dosing regimens, as shown in Figure 5 and 6. An accurate measurement of the mTFPI baseline in animals may further improve model predictive performance. As shown in Figure S4. increasing the rabbit mTFPI baseline 1.4 fold further improved model prediction of concizumab in rabbits.

3.5. Sensitivity analysis of the systems PK/PD model

A local sensitivity analysis was performed at a low dose of 0.25 mg/kg and a high dose of 9 mg/kg in humans for assessing the sensitivity of parameters pertaining to the linear pathway and the non-linear pathway to antibody clearance and sTFPI suppression. As shown in Figure 7, each simulation was done by increasing or decreasing the chosen parameter 10-fold from the value listed in Table 2. In Figure 7A, the most critical parameters for antibody clearance at the low dose were the turnover rate and baseline of mTFPI (k_{degm} and $mTFPI\_b$), which jointly define the capacity of the non-linear clearance pathway. A decrease in these two parameters increased the AUC of total antibody and thus decreased the AUC of free sTFPI. As is known for TMDD, the turnover rate and baseline of mTFPI have smaller effects on antibody clearance at the high dose (Figure 7B) than at the low dose (Figure 7A). The parameters associated with the linear clearance pathway had increased effects on total antibody clearance at the high dose, including antibody-FcRn binding constants (k_{1on} and k_{1off}), FcRn concentration in endosomes ($FcRn\_b$), endosomal volume for the nonspecific pinocytosis (V_{e2}), nonspecific pinocytosis clearance (CL_{up}), and lysosomal catabolism rate (CL_e). The volume of the endosomes for the endocytosis of AmTFPI (V_{e1}) negligibly

affected the AUCs of free sTFPI and total antibodies at the selected settings. Because the capacity of the non-linear mTFPI pathway ($mTFPI\_b \times k_{degm}$) is 12-fold larger than the linear sTFPI pathway ($sTFPI\_b \times k_{degs}$), the turnover of sTFPI (k_{degs}) had small effects on the AUC of total antibody at both doses. In line with that, the effects of antibody-mTFPI/sTFPI binding constants k_{on} and k_{off} on AUCs of free sTFPI and total antibody were smaller at the high dose than at the low dose when the high-capacity non-linear pathway dominates antibody disposition.

4. Discussion

Concizumab, an antibody that targets both mTFPI and sTFPI, is currently under phase II clinical investigation for treatment of hemophilia. Like other anti-TFPI antibodies (Gu et al., 2017; Parng et al., 2018), concizumab exhibits dose-dependent, non-linear PK that is mediated by binding to mTFPI. Due to the significant mTFPI-mediated non-linear clearance, high doses and frequent dosing of concizumab are needed to suppress sTFPI for hemophilia treatment.

Few empirical two-compartment models have been developed for anti-TFPI antibodies, including concizumab (Agerso et al., 2014; Gu et al., 2017; Parng et al., 2018). One empirical two-compartment model for concizumab applied Michaelis-Menten (MM) approximation to describe the TMDD of concizumab in monkeys (Agerso et al., 2014). However, it had no function for predicting the suppression of sTFPI. The model for BAY1093884 used quasi-equilibrium steady state (QSS) approximation to relate the turnover of sTFPI and the non-linear clearance of antibody (Gu et al., 2017), although sTFPI is not the driver for the non-linear clearance. The model for PF-06741086 is a hybrid model, using QSS approximation to describe sTFPI suppression and MM approximation to define the non-linear clearance of antibody (Parng et al., 2018). While these models can capture the PK and PD profiles of existing anti-TFPI antibodies, these models cannot be extrapolated to anti-TFPI recycling antibodies that show different binding kinetics in plasma and endosomes, which are of development interests for improving the dosing regimen of hemophilia treatment.

Our goal of this study was to develop a quantitative platform to explore the PK/PD of anti-TFPI recycling antibodies based on existing concizumab data and our current understanding of the TFPI biology. The ideal model should separately describe mTFPI and sTFPI dynamics for predicting the mTFPI-mediated non-linear clearance of concizumab and the suppressive effect on sTFPI, allowing extrapolation to species with potential different target kinetics. The ideal model should also incorporate the function to simulate altered endosomal target binding kinetics and the resulted change in the PK and PD. Toward this end, we developed a systems PK/PD model by extending our prior general model for recycling antibodies against soluble targets with a second endosome compartment for mTFPI-mediated TMDD, thus the dynamics of antibody bound to each target can be separately described. In each endosome compartment, antibody-target binding and FcRn-mediated recycling of antibodies were described for comparing the PK/PD of conventional antibodies and recycling antibodies from a mechanistic perspective.

Strategically, we designed a reduced PK/PD model without the endosome compartments to optimize the unknown turnover parameters for the mTFPI target and *in vivo* target binding kinetics in humans. To improve parameter identifiability, the final selected model fixed CL_{linear} to the clearance of a linearly cleared antibody, fixed k_{degs} to clinical observation, fixed k_{on} to *in vitro* measurement, and assumed $k_{degm} = k_{int}$. Parameter identifiability was improved by fixing k_{on} to *in vitro* measurement because the antibody-target binding kinetics. especially k_{on}, is much faster than other antibody disposition process and the current PK sampling schedules often do not allow identification of the antibody-target binding kinetics (Gibiansky and Gibiansky. 2009). $k_{degm} = k_{int}$ is typically assumed to improve parameter identifiability because such assumption ensures that the introduction of drug won't affect the turnover of the membrane target (Gibiansky and Gibiansky. 2009). thus reduces the complexity.

The optimized parameter values were then integrated into the systems PK/PD model for simulation in humans. The systems PK/PD model adequately predicted the plasma concentrations of total antibody and free sTFPI after IV and SC administration of concizumab in humans. Most model predictions for total antibody and sTFPI concentrations were within two standard deviations of observations. We believe that the two standard deviations of model predictions from observations could be tolerated given the intended application of the developed model. which is to guide antibody engineering in the early stage of drug development.

Applying the systems PK/PD model, we simulated anti-TFPI recycling antibodies in humans by altering the antibody association (k_{eon}) or dissociation (k_{eoff}) rate constants with mTFPI and sTFPI in the endosomes. Our prior model for recycling antibodies against soluble targets showed that k_{eoff} plays a greater role than k_{eon} in determining the extent of free antibody recycling to the plasma (Yuan et al., 2018). Consistent with this result, as shown in Figure 3, an increase in k_{eoff} had a greater effect than a decrease in k_{eon} on reducing antibody clearance and extending sTFPI suppression. Our prior model also showed that a further decrease in the target dissociation time ($1/k_{eoff}$) in endosomes beyond the endosomal transit time (11.5 min) had a decreased effect in soluble antigen suppression (Yuan et al., 2018). In Figure 3, however, a further decrease in the endosomal TFPI dissociation time ($1/k_{eoff}$) from 0.95 min (10-fold) to 0.095 min (100-fold) greatly extended the antibody circulation and sTFPI suppression. This discrepancy arose because the clearance of antibodies in our prior model was not affected by target release in the endosomes under the assumption that the antibody-soluble target complexes can still be recycled by FcRn (Yuan et al., 2018). Thus, the suppression of soluble targets in the prior model would reach a maximum when all targets can be released within the endosome transit time. In contrast, the clearance of anti-TFPI recycling antibodies was affected by mTFPI release in the endosomes, which decreased the non-linear clearance of the antibody and subsequently enhanced sTFPI suppression. Based on the simulations, a single IV administration of an anti-TFPI recycling antibody with a 100-fold increase in endosomal target dissociation rate constant (k_{eoff}) can suppress sTFPI below the LLOQ for a month at 3 mg/kg, compared to 12 days for concizumab at the same dose. The simulation results suggested that anti-TFPI recycling antibodies have a great potential in improving the dosing regimen for hemophilia treatment. Our simulation results provided a tentative affinity goal for antibody engineering: a 100-fold

higher target dissociation rate constant than concizumab at endosomal condition should be targeted. Given the antibody-target binding kinetics at endosomal condition and plasma condition which can be measured *in vitro*, we can predict the PK/PD and required dosing regimen for each anti-TFPI recycling antibody. Without the modeling platform, each anti-TFPI recycling antibody needs to be tested empirically.

In addition, we were able to extrapolate the systems PK/PD model from humans to monkeys and rabbits, two commonly used preclinical species in hemophilia study. The interspecies translation was done by parameterizing the same model structure with reported species-specific physiological parameters, sTFPI baselines, and parameters optimized using PK data of other antibodies. The obtained systems PK/PD model adequately captured the plasma profiles of concizumab in monkeys and rabbits in different dosing regimens. By bridging the three animal species, the systems PK/PD model can serve as a quantitative platform for facilitating the preclinical and translational development of anti-TFPI recycling antibodies.

Several model assumptions were made for the systems PK/PD model. Like our prior model (Yuan et al., 2018), AsTFPI was assumed to bind FcRn with the same binding affinity as free antibodies. The antibody-FcRn binding affinities, FcRn concentrations in endosomes, and endosome trafficking kinetics like k_{rec} were assumed to be preserved across species. Like other TMDD models (Gibiansky and Gibiansky, 2010), our model assumed stable target turnover for mTFPI and sTFPI. However, it has been reported in mice that the inhibitory effect of anti-TFPI antibodies on bleeding progressively decreased at doses greater than the amount needed to neutralize sTFPI, suggesting that a sequestered pool of TFPI, likely from platelets and endothelial cells, could be released (Broze and Girard, 2012; Maroney et al., 2012). High inter-individual variability in concizumab PK was observed in monkeys, as shown in Figure 5. This may relate to the inter-individual variability in target homeostasis and regulation. In addition, we didn't distinguish the different isoforms of sTFPI and assumed that concizumab had equal binding affinity to mTFPI and sTFPI because concizumab targets the shared K2 domain. However, the binding affinity of concizumab to mTFPI and different isoforms of sTFPI may vary within each species. Species differences in mTFPI and sTFPI baselines were considered, but those related to binding affinities were not. Nonetheless, target binding affinities only have small effects on plasma concentrations of total antibodies and free sTFPI, as indicated by the local sensitivity analysis.

Compared with the prior empirical models (Agerso et al., 2014; Gu et al., 2017; Parng et al., 2018), our systems PK/PD model included more mechanistic components for describing the two clearance pathways of anti-TFPI antibodies and for predicting the PK/PD advantage of anti-TFPI recycling antibodies in comparison with concizumab, allowing integrating of *in vitro* measured parameters. Like other systems model, many model assumptions were made to improve parameter identifiability. As a part of the "learn and confirm" drug development paradigm, the systems PK/PD model can be further optimized upon data for anti-TFPI recycling antibodies and experimental measurements of model parameters become available.

5. Conclusion

We developed a systems PK/PD model that mechanistically described the PK/PD of concizumab in humans, monkeys, and rabbits. This systems PK/PD model predicted that anti-TFPI recycling antibodies can improve the dosing regimen for hemophilia treatment. As a quantitative platform, the systems PK/PD model can facilitate the development of anti-TFPI recycling antibodies by setting the affinity goal and bridging three animal species.

Supplementary Material

Refer to Web version on PubMed Central for supplementary material.

Acknowledgments

This work was supported by the National Institutes of General Medical Sciences [R35 GM119661]. The authors thank the RxODE development team for their expertise in this R package.

Appendix

8.

8. Appendix I:: a glossary of parameters in the systems PK/PD model

Parameter	Definition
Physiological parameters	
V_p	Plasma volume (L)
V_{isf}	Volume of interstitial fluid (L); $V_{isf} = V_1 + V_2$
V_1	Interstitial space of tissues with continuous vessels (tight tissues, including brain, muscle, skin, adipose); $V_1 = 0.65 \cdot V_{isf}$ (Cao et al., 2013)
V_2	Interstitial space of tissues with leaky vessels (leaky tissues, including liver, kidney, heart, etc.); $V_2 = 0.35 \cdot V_{isf}$ (Cao et al., 2013)
K_p	Fraction of interstitial space available for antibody distribution (0.8 for native IgG_1, 0.4 for native IgG_4) (Cao et al., 2013)
V_l	Volume of lymph (L)
L	Total lymph flow ($L \cdot day^{-1}$); $L = L_1 + L_2$
L_1	Lymph flow from tight tissues ($L \cdot day^{-1}$); $L_1 = 0.33L$ (Cao et al., 2013)
L_2	Lymph flow from leaky tissues ($L \cdot day^{-1}$); $L_2 = 0.67$ L (Cao et al., 2013)
σ_1	Vascular reflection coefficient for tight tissues, reflect the level of resistance to antibody convection provided by continuous vessels
σ_2	Vascular reflection coefficient for leaky tissues, reflect the level of resistance to antibody convection provided by leaky vessels, $\sigma_2 < \sigma_1$
σ_l	Lymphatic vascular reflection coefficient, reflect the level of resistance to antibody convection provided by lymph vessels
Endosome parameters	
CL_{up}	Endothelial nonspecific pinocytosis rate ($L \cdot day^{-1}$)
k_{rec}	Endosome recycling rate constant (day^{-1})
CL_e	Lysosome catabolism clearance ($L \cdot day^{-1}$)

Parameter	Definition
V_{e1}	Endosome volume for receptor (mTFPI)-mediated endocytosis
V_{e2}	Endosome volume for nonspecific pinocytosis
$FcRn\_b$	FcRn baseline concentration in endosomes (μM)
k_{1on}	Antibody FcRn association rate constant ($M^{-1}{\cdot}s^{-1}$) in endosomes
k_{1off}	Antibody-FcRn complex (FcRnA) dissociation rate constant (s^{-1}) in endosomes
Target (mTFPI and sTFPI) parameters	
k_{on}	Antibody TFPI association rate constant ($M^{-1}{\cdot}s^{-1}$) in plasma
k_{off}	Antibody-TFPI complex dissociation rate constant (s^{-1}) in plasma
k_{eon}	Antibody TFPI association rate constant ($M^{-1}{\cdot}s^{-1}$) in endosomes
k_{eoff}	Antibody-TFPI complex dissociation rate constant (s^{-1}) in endosomes
$sTFPI\_b$	sTFPI baseline concentration in plasma (nM)
k_{syns}	Zero order synthesis rate of sTFPI ($nM{\cdot}day^{-1}$)
k_{degs}	1st order total degradation rate constant of sTFPI (day^{-1})
$k_{degs'}$	1st order nonspecific pinocytosis-independent degradation rate constant of sTFPI (day^{-1}), such as kidney filtration, enzymatic degradation in plasma, etc.
$mTFPI\_b$	mTFPI baseline concentration on endothelial cell surface (nM)
k_{synm}	Zero order synthesis rate of mTFPI ($nM{\cdot}day^{-1}$)
k_{degm}	Endothelial cell internalization rate constant of free mTFPI (day^{-1})
k_{int}	Endothelial cell internalization rate constant of mTFPI-bound antibody (AmTFPI)(day^{-1})
Other parameters	
F	SC bioavailability of concizumab
k_a	SC 1st order absorption rate constant of concizumab (day^{-1})
CL_{linear}	Linear clearance of antibody and soluble complex

8. Appendix II:: model equations and initial conditions (IC) for the systems PK/PD model of anti-TFPI antibodies

Antibody amount in SC absorption depot compartment

$$\frac{d(depot)}{dt} = -depot \cdot k_a; \qquad IC(depot) = F \cdot Dose \tag{1}$$

Concentration of free antibody (A) in plasma V_p

$$\frac{d(A_p)}{dt} = \frac{k_a \cdot depot \cdot switcher}{V_p} - k_{on} \cdot A_p \cdot sTFPI_p + k_{off} \cdot AsTFPI_p - k_{on} \cdot A_p \cdot mTFPI_p + k_{off} \cdot AmTFPI_p - \frac{(1-\sigma_1) \cdot L_1 \cdot A_p}{V_p} - \frac{(1-\sigma_2) \cdot L_2 \cdot A_p}{V_p} + \frac{L \cdot A_l}{V_p} - \frac{CL_{up} \cdot A_p}{V_p} + \frac{k_{rec} \cdot (FcRnA_{e1} \cdot V_{e1} + FcRnA_{e2} \cdot V_{e2})}{V_p}; \quad (2)$$

$$IC(A_p) = Dose/V_p \cdot (1 - switcher); switcher = 0 \; for \; IV, \; switcher = 1 \; for \; SC$$

Concentration of free sTFPI in plasma V_p

$$\frac{d(sTFPI_p)}{dt} = -k_{on} \cdot A_p \cdot sTFPI_p + k_{off} \cdot AsTFPI_p + k_{syns} - k'_{degs} \cdot sTFPI_p - \frac{CL_{up} \cdot sTFPI_p}{V_p}, \quad (3)$$

$$k_{syns} = k_{degs} \cdot sTFPI\_b;$$

$$k'_{degs} = k_{degs} - \frac{CL_{up}}{v_p};$$

$$IC(sTFPI_p) = sTFPI\_b$$

Concentration of antibody-sTFPI (AsTFPI) complex in plasma V_p

$$\frac{d(AsTFPI_p)}{dt} = k_{on} \cdot A_p \cdot sTFPI_p - k_{off} \cdot AsTFPI_p - \frac{(1-\sigma_1) \cdot L_1 \cdot AsTFPI_p}{V_p} - \frac{(1-\sigma_2) \cdot L_2 \cdot AsTPFI_p}{V_p} + \frac{L \cdot AsTFPI_l}{V_p} - \frac{CL_{up} \cdot AsTFPI_p}{V_p} + \frac{k_{rec} \cdot FcRnAsTFPI_{e2} \cdot V_{e2}}{V_p}; \quad (4)$$

$$IC(AsTFPI_p) = 0$$

Concentration of free mTFPI in plasma V_p

$$\frac{d\left(mTFPI_p\right)}{dt} = -k_{on}\cdot A_p\cdot mTFPI_p + k_{off}\cdot AmTFPI_p + k_{synm} - k_{degm} \cdot mTFPI_p;$$
$$k_{synm} = k_{degm}\cdot mTFPI\_b;$$
$$IC\left(mTFPI_p\right) = mTFPI\_b \quad (5)$$

Concentration of antibody-mTFPI complex (AmTFPI) in plasma V_p

$$\frac{d\left(AmTFPI_p\right)}{dt} = k_{on}\cdot A_p\cdot mTFPI_p - k_{off}\cdot AmTFPI_p - k_{int}\cdot AmTFPI_p;$$
$$IC\left(AmTFPI_p\right) = 0 \quad (6)$$

Concentration of free antibody in the endosome of mTFPI-mediated endocytosis V_{e1}

$$\frac{d\left(A_{e1}\right)}{dt} = -k_{eon}\cdot A_{e1}\cdot mTFPI_{e1} + k_{eoff}\cdot AmTFPI_{e1} - k_{1on}\cdot A_{e1}\cdot FcRn_{e1} + k_{1off}\cdot FcRnA_{e1} - \frac{CL_e\cdot A_{e1}}{V_{e1}};$$
$$IC\left(A_{e1}\right) = 0 \quad (7)$$

Concentration of free mTFPI in the endosome of mTFPI-mediated endocytosis V_{e1}

$$\frac{d\left(mTFPI_{e1}\right)}{dt} = -k_{eon}\cdot A_{e1}\cdot mTFPI_{e1} + k_{eoff}\cdot AmTFPI_{e1} + \frac{k_{degm}\cdot mTFPI_p\cdot V_p}{V_{e1}} - \frac{CL_e\cdot mTFPI_{e1}}{V_{e1}};$$
$$IC\left(mTFPI_{e1}\right) = \frac{mTFPI\_b\cdot k_{degm}\cdot V_p}{CL_e} \quad (8)$$

Concentration of antibody-mTFPI complex (AmTFPI) in the endosome of mTFPI-mediated endocytosis V_{e1}

$$\frac{d(AmTFPI_{e1})}{dt} = k_{eon} \cdot A_{e1} \cdot mTFPI_{e1} - k_{eoff} \cdot AmTFPI_{e1} + \frac{k_{int} \cdot AmTFPI_p \cdot V_p}{V_{e1}}; \quad (9)$$
$$IC(AmTFPI_{e1}) = 0$$

Concentration of free FcRn in the endosome of mTFPI-mediated endocytosis V_{e1}

$$\frac{d(FcRn_{e1})}{dt} = -k_{1on} \cdot FcRn_{e1} \cdot A_{e1} + k_{1off} \cdot FcRnA_{e1} + k_{rec} \cdot FcRnA_{e1}; \quad (10)$$
$$IC(FcRn_{e1}) = FcRn\_b$$

Concentration of Antibody-FcRn complex (FcRnA) in the endosome of mTFPI-mediated endocytosis V_{e1}

$$\frac{d(FcRnA_{e1})}{dt} = k_{1on} \cdot FcRn_{e1} \cdot A_{e1} - k_{1off} \cdot FcRnA_{e1} - k_{rec} \cdot FcRnA_{e1}; \quad (11)$$
$$IC(FcRnA_{e1}) = 0$$

Concentration of free antibody (A) in the endosome of nonspecific pinocytosis V_{e2}

$$\frac{d(A_{e2})}{dt} = -k_{1on} \cdot A_{e2} \cdot FcRn_{e2} + k_{1off} \cdot FcRnA_{e2} - k_{eon} \cdot A_{e2} \cdot sTFPI_{e2} + k_{eoff} \cdot AsTFPI_{e2} - \frac{CL_e \cdot A_{e2}}{V_{e2}} + \frac{CL_{up} \cdot A_p}{V_{e2}}; \quad (12)$$
$$IC(A_{e2}) = 0$$

Concentration of free sTFPI in the endosome of nonspecific pinocytosis V_{e2}

$$\frac{d(sTFPI_{e2})}{dt} = -k_{eon} \cdot FcRnA_{e2} \cdot sTFPI_{e2} + k_{eoff} \cdot FcRnAsTFPI_{e2} - k_{eon} \cdot A_{e2} \cdot sTFPI_{e2} + k_{eoff} \cdot AsTFPI_{e2} - \frac{CL_e \cdot sTFPI_{e2}}{V_{e2}} + \frac{CL_{up} \cdot sTFPI_p}{V_{e2}}; \quad (13)$$
$$IC(sTFPI_{e2}) = \frac{sTFPI\_b \cdot CL_{up}}{CL_e}$$

Concentration of antibody-sTFPI complex (AsTFPI) in the endosome of nonspecific pinocytosis V_{e2}

$$\frac{d(AsTFPI_{e2})}{dt} = -k_{1on} \cdot AsTFPI_{e2} \cdot FcRn_{e2} + k_{1off} \cdot FcRnAsTFPI_{e2} + k_{eon} \cdot A_{e2} \cdot sTFPI_{e2} - k_{eoff} \cdot AsTFPI_{e2} - \frac{CL_e \cdot AsTFPI_{e2}}{V_{e2}} + \frac{CL_{up} \cdot AsTFPI_p}{V_{e2}}; \quad (14)$$

$$IC(AsTFPI_{e2}) = 0$$

Concentration of free FcRn in the endosome of nonspecific pinocytosis V_{e2}

$$\frac{d(FcRn_{e2})}{dt} = -k_{1on} \cdot A_{e2} \cdot FcRn_{e2} + k_{1off} \cdot FcRnA_{e2} - k_{1on} \cdot AsTFPI_{e2} \cdot FcRn_{e2} + k_{1off} \cdot FcRnAsTFPI_{e2} + k_{rec} \cdot (FcRnA_{e2} + FcRnAsTFPI_{e2}); \quad (15)$$

$$IC(FcRn_{e2}) = FcRn\_b$$

Concentration of antibody-FcRn complex (FcRnA) in the endosome of nonspecific pinocytosis V_{e2}

$$\frac{d(FcRnA_{e2})}{dt} = k_{1on} \cdot A_{e2} \cdot FcRn_{e2} - k_{1off} \cdot FcRnA_{e2} - k_{eon} \cdot FcRnA_{e2} \cdot sTFPI_{e2} + k_{eoff} \cdot FcRnAsTFPI_{e2} - k_{rec} \cdot FcRnA_{e2}; \quad (16)$$

$$IC(FcRnA_{e2}) = 0$$

Concentration of FcRn-bound AsTFPI complex (FcRnAsTFPI) in the endosome of nonspecific pinocytosis V_{e2}

$$\frac{d(FcRnAsTFPI_{e2})}{dt} = k_{1on} \cdot AsTFPI_{e2} \cdot FcRn_{e2} - k_{1off} \cdot FcRnAsTFPI_{e2} + k_{eon} \cdot FcRnA_{e2} \cdot sTFPI_{e2} - k_{eoff} \cdot FcRnAsTFPI_{e2} - k_{rec} \cdot FCRnAsTFPI_{e2}; \quad (17)$$

$$IC(FcRnAsTFPI_{e2}) = 0$$

Concentration of free antibody (A) in tight tissue V_1

$$\frac{d(A_1)}{dt} = \frac{(1-\sigma_1) \cdot L_1 \cdot A_p - (1-\sigma_l) \cdot L_1 \cdot A_1}{V_1 \cdot K_p}; \quad (18)$$

$$IC(A_1) = 0$$

Concentration of free antibody-sTFPI complex (AsTFPI) in tight tissue V_1

$$\frac{d(AsTFPI_1)}{dt} = \frac{(1-\sigma_1)\cdot L_1 \cdot AsTFPI_p - (1-\sigma_l)\cdot L_1 \cdot AsTFPI_1}{V_1 \cdot K_p};$$
$$IC(AsTFPI_1) = 0 \tag{19}$$

Concentration of free antibody (A) in leaky tissue V_2

$$\frac{d(A_2)}{dt} = \frac{(1-\sigma_2)\cdot L_2 \cdot A_p - (1-\sigma_l)\cdot L_2 \cdot A_2}{V_2 \cdot K_p};$$
$$IC(A_2) = 0 \tag{20}$$

Concentration of antibody-sTFPI complex (AsTFPI) in leaky tissue V_2

$$\frac{d(AsTFPI_2)}{dt} = \frac{(1-\sigma_2)\cdot L_2 \cdot AsTFPI_p - (1-\sigma_l)\cdot L_2 \cdot AsTFPI_2}{V_2 \cdot K_p};$$
$$IC(AsTFPI_2) = 0 \tag{21}$$

Concentration of free antibody (A) in lymph V_l

$$\frac{d(A_l)}{dt} = \frac{(1-\sigma_l)\cdot L_1 \cdot A_1}{V_l} + \frac{(1-\sigma_l)\cdot L_2 \cdot A_2}{V_l} - \frac{L \cdot A_l}{V_l};$$
$$IC(A_l) = 0 \tag{22}$$

Concentration of antibody-sTFPI complex (AsTFPI) in lymph V_l

$$\frac{d(AsTFPI_l)}{dt} = \frac{(1-\sigma_l)\cdot L_1 \cdot AsTFPI_1}{V_l} + \frac{(1-\sigma_l)\cdot L_2 \cdot AsTFPI_2}{V_l} - \frac{L \cdot AsTFPI_l}{V_l};$$
$$IC(AsTFPI_l) = 0 \tag{23}$$

8. Appendix III:: model equations and initial conditions (IC) for the reduced PK/PD model of anti-TFPI antibodies

The plasma compartment of the reduced PK/PD model for concizumab is described by Equation (24–28) in below. The equations for the compartments of tight tissues, leaky

tissues, and lymph in the reduced model remain the same as the systems PK/PD model (Equations (18–23)).

Concentration of free antibody in plasma V_p

$$\frac{d(A_p)}{dt} = -k_{on}\cdot A_p\cdot sTFPI_p + k_{off}\cdot AsTFPI_p - k_{on}\cdot A_p\cdot mTFPI_p + k_{off}\cdot AmTFPI_p - \frac{(1-\sigma_1)\cdot L_1\cdot A_p}{V_p} - \frac{(1-\sigma_2)\cdot L_2\cdot A_p}{V_p} + \frac{L\cdot A_l}{V_p} - \frac{CL_{linear}\cdot A_p}{V_p}; \quad (24)$$

$$IC(A_p) = \frac{Dose}{V_p}$$

Concentration of free sTFPI in plasma V_p

$$\frac{d(sTFPI_p)}{dt} = -k_{on}\cdot A_p\cdot sTFPI_p + k_{off}\cdot AsTFPI_p + k_{syns} - k_{degs}\cdot sTFPI_p; \quad (25)$$

$$k_{syns} = k_{degs}\cdot sTFPI\_b;$$

$$IC(sTFPI_p) = sTFPI\_b$$

Concentration of antibody-sTFPI complex (AsTFPI) in plasma V_p

$$\frac{d(AsTFPI_p)}{dt} = k_{on}\cdot A_p\cdot sTFPI_p - k_{off}\cdot AsTFPI_p - \frac{(1-\sigma_1)\cdot L_1\cdot AsTFPI_p}{V_p} - \frac{(1-\sigma_2)\cdot L_2\cdot AsTFPI_p}{V_p} + \frac{L\cdot AsTFPI_l}{V_p} - \frac{CL_{linear}\cdot AsTFPI_p}{V_p}; \quad (26)$$

$$IC(AsTFPI_p) = 0$$

Concentration of free mTFPI in plasma V_p

$$\frac{d(mTFPI_p)}{dt} = -k_{on}\cdot A_p\cdot mTFPI_p + k_{off}\cdot AmTFPI_p + k_{synm} - k_{degm}\cdot mTFPI_p; \quad (27)$$

$$k_{synm} = k_{degm}\cdot mTFPI\_b;$$

$$IC(mTFPI_p) = mTFPI\_b$$

Concentration of antibody-mTFPI complex (AmTFPI) in plasma V_p

$$\frac{d\left(AmTFPI_p\right)}{dt} = k_{on} \cdot A_p \cdot mTFPI_p - k_{off} \cdot AmTFPI_p - k_{int} \cdot AmTFPI_p;$$
$$IC\left(AmTFPI_p\right) = 0 \quad (28)$$

References

Agerso H, Overgaard RV, Petersen MB, Hansen L, Hermit MB, Sorensen MH, Petersen LC, Hilden I, 2014 Pharmacokinetics of an anti-TFPI monoclonal antibody (concizumab) blocking the TFPI interaction with the active site of FXa in Cynomolgus monkeys after iv and sc administration. Eur J Pharm Sci 56, 65–69. [PubMed: 24568891]

al, A.S.e.m., 2018 DescTools: Tools for descriptive statistics. R package version 0.99.24.

Armin J, Grant RT, Pels H, Reeve EB, 1952 The plasma, cell and blood volumes of albino rabbits as estimated by the dye (T 1824) and 32P marked cell methods. J Physiol 116, 59–73. [PubMed: 14898538]

Betts A, Keunecke A, van Steeg TJ, van der Graaf PH, Avery LB, Jones H, Berkhout J, 2018 Linear pharmacokinetic parameters for monoclonal antibodies are similar within a species and across different pharmacological targets: A comparison between human, cynomolgus monkey and hFcRn Tg32 transgenic mouse using a population-modeling approach. MAbs 10, 751–764. [PubMed: 29634430]

Broze GJ Jr., Girard TJ, 2012 Tissue factor pathway inhibitor: structure-function. Front Biosci (Landmark Ed) 17, 262–280. [PubMed: 22201743]

Cao Y, Balthasar JP, Jusko WJ, 2013 Second-generation minimal physiologically-based pharmacokinetic model for monoclonal antibodies. J Pharmacokinet Pharmacodyn 40, 597–607. [PubMed: 23996115]

Cao Y, Jusko WJ, 2014 Survey of monoclonal antibody disposition in man utilizing a minimal physiologically-based pharmacokinetic model. J Pharmacokinet Pharmacodyn 41, 571–580. [PubMed: 25146360]

Chen Y, Balthasar JP, 2012 Evaluation of a catenary PBPK model for predicting the in vivo disposition of mAbs engineered for high-affinity binding to FcRn. AAPS J 14, 850–859. [PubMed: 22956476]

Chowdary P, Lethagen S, Friedrich U, Brand B, Hay C, Abdul Karim F, Klamroth R, Knoebl P, Laffan M, Mahlangu J, Miesbach W, Dalsgaard Nielsen J, Martin-Salces M, Angchaisuksiri P, 2015 Safety and pharmacokinetics of anti-TFPI antibody (concizumab) in healthy volunteers and patients with hemophilia: a randomized first human dose trial. J Thromb Haemost 13, 743–754. [PubMed: 25641556]

D'Argenio DZ, Schumitzky A, Wang X, 2009 ADAPT 5 User's Guide: Pharmacokinetic/Pharmacodynamic Systems Analysis Software. Biomedical Simulation Resource, Los Angeles.

Diao L, Meibohm B, 2015 Tools for predicting the PK/PD of therapeutic proteins. Expert Opin Drug Metab Toxicol 11, 1115–1125. [PubMed: 25936400]

Dostalek M, Gardner I, Gurbaxani BM, Rose RH, Chetty M, 2013 Pharmacokinetics, pharmacodynamics and physiologically-based pharmacokinetic modelling of monoclonal antibodies. Clin Pharmacokinet 52, 83–124. [PubMed: 23299465]

Duckers C, Simioni P, Spiezia L, Radu C, Gavasso S, Rosing J, Castoldi E, 2008 Low plasma levels of tissue factor pathway inhibitor in patients with congenital factor V deficiency. Blood 112, 3615–3623. [PubMed: 18695002]

Eichler H, Angchaisuksiri P, Kavakli K, Knoebl P, Windyga J, Jimenez-Yuste V, Hyseni A, Friedrich U, Chowdary P, 2018 A randomized trial of safety, pharmacokinetics and pharmacodynamics of concizumab in people with hemophilia A. J Thromb Haemost 16, 2184–2195. [PubMed: 30137664]

Farrokhi V, Chen X, Neubert H, 2018 Protein Turnover Measurements in Human Serum by Serial Immunoaffinity LC-MS/MS. Clinical chemistry 64, 279–288. [PubMed: 29054922]

Gibiansky L, Gibiansky E, 2009 Target-mediated drug disposition model: approximations, identifiability of model parameters and applications to the population pharmacokinetic-pharmacodynamic modeling of biologics. Expert Opin Drug Metab Toxicol 5, 803–812. [PubMed: 19505189]

Gibiansky L, Gibiansky E, 2010 Target-mediated drug disposition model for drugs that bind to more than one target. J Pharmacokinet Phar 37, 323–346.

Ginestet C, 2011 ggplot2: Elegant Graphics for Data Analysis. J R Stat Soc a Stat 174, 245–245.

Gu JM, Zhao XY, Schwarz T, Schuhmacher J, Baumann A, Ho E, Subramanyan B, Tran K, Myles T, Patel C, Koellnberger M, 2017 Mechanistic Modeling of the Pharmacodynamic and Pharmacokinetic Relationship of Tissue Factor Pathway Inhibitor-Neutralizing Antibody (BAY 1093884) in Cynomolgus Monkeys. AAPS J 19, 1186–1195. [PubMed: 28516358]

Hansen L, Petersen LC, Lauritzen B, Clausen JT, Grell SN, Agerso H, Sorensen BB, Hilden I, Almholt K, 2014 Target-mediated clearance and bio-distribution of a monoclonal antibody against the Kunitz-type protease inhibitor 2 domain of Tissue Factor Pathway Inhibitor. Thromb Res 133, 464–471. [PubMed: 24393663]

Hilden I, Lauritzen B, Sorensen BB, Clausen JT, Jespersgaard C, Krogh BO, Bowler AN, Breinholt J, Gruhler A, Svensson LA, Petersen HH, Petersen LC, Balling KW, Hansen L, Hermit MB, Egebjerg T, Friederichsen B, Ezban M, Bjorn SE, 2012 Hemostatic effect of a monoclonal antibody mAb 2021 blocking the interaction between FXa and TFPI in a rabbit hemophilia model. Blood 119, 5871–5878. [PubMed: 22563084]

Hironiwa N, Ishii S, Kadono S, Iwayanagi Y, Mimoto F, Habu K, Igawa T, Hattori K, 2016 Calcium-dependent antigen binding as a novel modality for antibody recycling by endosomal antigen dissociation. MAbs 8, 65–73. [PubMed: 26496237]

Hopkins CR, Trowbridge IS, 1983 Internalization and processing of transferrin and the transferrin receptor in human carcinoma A431 cells. J Cell Biol 97, 508–521. [PubMed: 6309862]

Igawa T, Ishii S, Tachibana T, Maeda A, Higuchi Y, Shimaoka S, Moriyama C, Watanabe T, Takubo R, Doi Y, Wakabayashi T, Hayasaka A, Kadono S, Miyazaki T, Haraya K, Sekimori Y, Kojima T, Nabuchi Y, Aso Y, Kawabe Y, Hattori K, 2010 Antibody recycling by engineered pH-dependent antigen binding improves the duration of antigen neutralization. Nat Biotechnol 28, 12031207.

Igawa T, Mimoto F, Hattori K, 2014 pH-dependent antigen-binding antibodies as a novel therapeutic modality. Biochim Biophys Acta 1844, 1943–1950. [PubMed: 25125373]

Jolles S, Sewell WA, Misbah SA, 2005 Clinical uses of intravenous immunoglobulin. Clin Exp Immunol 142, 1–11. [PubMed: 16178850]

Krippendorff BF, Kuester K, Kloft C, Huisinga W, 2009 Nonlinear pharmacokinetics of therapeutic proteins resulting from receptor mediated endocytosis. J Pharmacokinet Pharmacodyn 36, 239–260. [PubMed: 19554432]

Kuo TT, Aveson VG, 2011 Neonatal Fc receptor and IgG-based therapeutics. MAbs 3, 422–430. [PubMed: 22048693]

Latvala S, Jacobsen B, Otteneder MB, Herrmann A, Kronenberg S, 2017 Distribution of FcRn Across Species and Tissues. J Histochem Cytochem 65, 321–333. [PubMed: 28402755]

Li L, Gardner I, Dostalek M, Jamei M, 2014 Simulation of monoclonal antibody pharmacokinetics in humans using a minimal physiologically based model. AAPS J 16, 1097–1109. [PubMed: 25004823]

Li Z, Krippendorff BF, Shah DK, 2017 Influence of Molecular size on the clearance of antibody fragments. Pharm Res 34, 2131–2141. [PubMed: 28681164]

Mager DE, 2006 Target-mediated drug disposition and dynamics. Biochem Pharmacol 72, 1–10. [PubMed: 16469301]

Maroney SA, Cooley BC, Ferrel JP, Bonesho CE, Nielsen LV, Johansen PB, Hermit MB, Petersen LC, Mast AE, 2012 Absence of hematopoietic tissue factor pathway inhibitor mitigates bleeding in mice with hemophilia. Proc Natl Acad Sci U S A 109, 3927–3931. [PubMed: 22355108]

Maroney SA, Ellery PE, Mast AE, 2010 Alternatively spliced isoforms of tissue factor pathway inhibitor. Thromb Res 125 Suppl 1, S52–56. [PubMed: 20176395]

Mayor S, Sabharanjak S, Maxfield FR, 1998 Cholesterol-dependent retention of GPI-anchored proteins in endosomes. EMBO J 17, 4626–4638. [PubMed: 9707422]

Neuber T, Frese K, Jaehrling J, Jager S, Daubert D, Felderer K, Linnemann M, Hohne A, Kaden S, Kolln J, Tiller T, Brocks B, Ostendorp R, Pabst S, 2014 Characterization and screening of IgG binding to the neonatal Fc receptor. MAbs 6, 928–942. [PubMed: 24802048]

Oitate M, Masubuchi N, Ito T, Yabe Y, Karibe T, Aoki T, Murayama N, Kurihara A, Okudaira N, Izumi T, 2011 Prediction of human pharmacokinetics of therapeutic monoclonal antibodies from simple allometry of monkey data. Drug Metab Pharmacokinet 26, 423–430. [PubMed: 21606605]

Parng C, Singh P, Pittman DD, Wright K, Leary B, Patel-Hett S, Rakhe S, Stejskal J, Peraza M, Dufield D, Murphy JE, Webster R, 2018 Title: Translational PK/PD characterization and TMDD modeling of an anti-TFPI antibody, PF-06741086. J Pharm Sci.

Pavlin DJ, Nessly ML, Haschke R, Cheney FW, 1986 Extracellular fluid volume during pneumothorax and hypoxemia in rabbits. J Appl Physiol (1985) 60, 204–208. [PubMed: 3080397]

Peterson JA, Maroney SA, Mast AE, 2016 Targeting TFPI for hemophilia treatment. Thromb Res 141 Suppl 2, S28–30. [PubMed: 27207418]

Rippe B, Haraldsson B, 1987 Fluid and protein fluxes across small and large pores in the microvasculature. Application of two-pore equations. Acta Physiol Scand 131, 411–428. [PubMed: 3321914]

Roopenian DC, Akilesh S, 2007 FcRn: the neonatal Fc receptor comes of age. Nat Rev Immunol 7, 715–725. [PubMed: 17703228]

Ryman JT, Meibohm B, 2017 Pharmacokinetics of Monoclonal Antibodies. CPT Pharmacometrics Syst Pharmacol 6, 576–588. [PubMed: 28653357]

Sampei Z, Haraya K, Tachibana T, Fukuzawa T, Shida-Kawazoe M, Gan SW, Shimizu Y, Ruike Y, Feng S, Kuramochi T, Muraoka M, Kitazawa T, Kawabe Y, Igawa T, Hattori K, Nezu J, 2018 Antibody engineering to generate SKY59, a long-acting anti-C5 recycling antibody. PLoS One 13, e0209509. [PubMed: 30592762]

Shah DK, Betts AM, 2012 Towards a platform PBPK model to characterize the plasma and tissue disposition of monoclonal antibodies in preclinical species and human. J Pharmacokinet Pharmacodyn 39, 67–86. [PubMed: 22143261]

Suzuki T, Ishii-Watabe A, Tada M, Kobayashi T, Kanayasu-Toyoda T, Kawanishi T, Yamaguchi T, 2010 Importance of neonatal FcR in regulating the serum half-life of therapeutic proteins containing the Fc domain of human IgG1: a comparative study of the affinity of monoclonal antibodies and Fc-fusion proteins to human neonatal FcR. J Immunol 184, 1968–1976. [PubMed: 20083659]

Szikora B, Hiripi L, Bender B, Kacskovics I, Ilias A, 2017 Characterization of the interactions of rabbit neonatal Fc receptor (FcRn) with rabbit and human IgG isotypes. PLoS One 12, e0185662. [PubMed: 28957416]

Vidarsson G, Dekkers G, Rispens T, 2014 IgG subclasses and allotypes: from structure to effector functions. Front Immunol 5, 520. [PubMed: 25368619]

Wang B, Lau YY, Liang M, Vainshtein I, Zusmanovich M, Lu H, Magrini F, Sleeman M, Roskos L, 2012 Mechanistic modeling of antigen sink effect for mavrilimumab following intravenous administration in patients with rheumatoid arthritis. J Clin Pharmacol 52, 1150–1161. [PubMed: 21947370]

Wang W, Hallow K, James D, 2016 A Tutorial on RxODE: Simulating Differential Equation Pharmacometric Models in R. CPT: Pharmacometrics & Systems Pharmacology 5, 3–10. [PubMed: 26844010]

Yeung YA, Wu X, Reyes AE 2nd, Vernes JM, Lien S, Lowe J, Maia M, Forrest WF, Meng YG, Damico LA, Ferrara N, Lowman HB, 2010 A therapeutic anti-VEGF antibody with increased potency independent of pharmacokinetic half-life. Cancer Res 70, 3269–3277. [PubMed: 20354184]

Yuan D, Rode F, Cao Y, 2018 A Minimal Physiologically Based Pharmacokinetic Model with a Nested Endosome Compartment for Novel Engineered Antibodies. AAPS J 20, 48. [PubMed: 29541870]

Zalevsky J, Chamberlain AK, Horton HM, Karki S, Leung IW, Sproule TJ, Lazar GA, Roopenian DC, Desjarlais JR, 2010 Enhanced antibody half-life improves in vivo activity. Nat Biotechnol 28, 157159.

Zhao J, Cao Y, Jusko WJ, 2015 Across-Species Scaling of Monoclonal Antibody Pharmacokinetics Using a Minimal PBPK Model. Pharm Res 32, 3269–3281. [PubMed: 25939552]

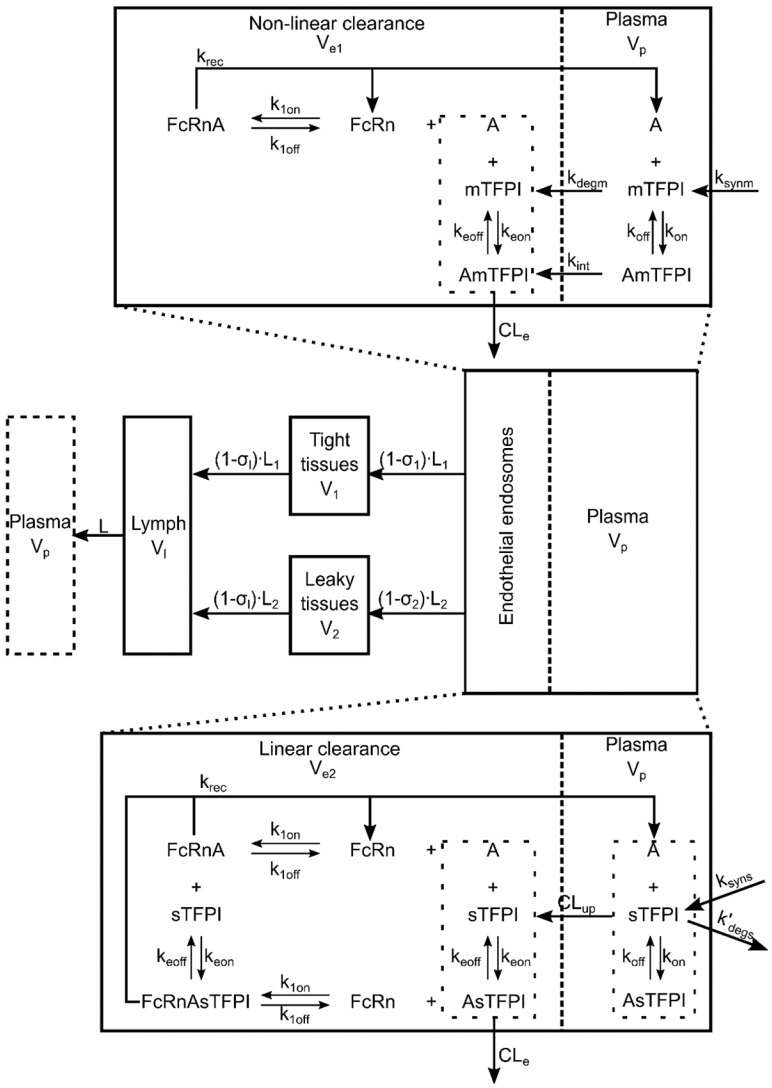

Figure 1.

Model structure of the systems PK/PD model for anti-TFPI antibodies. Model parameters are defined in Appendix I.

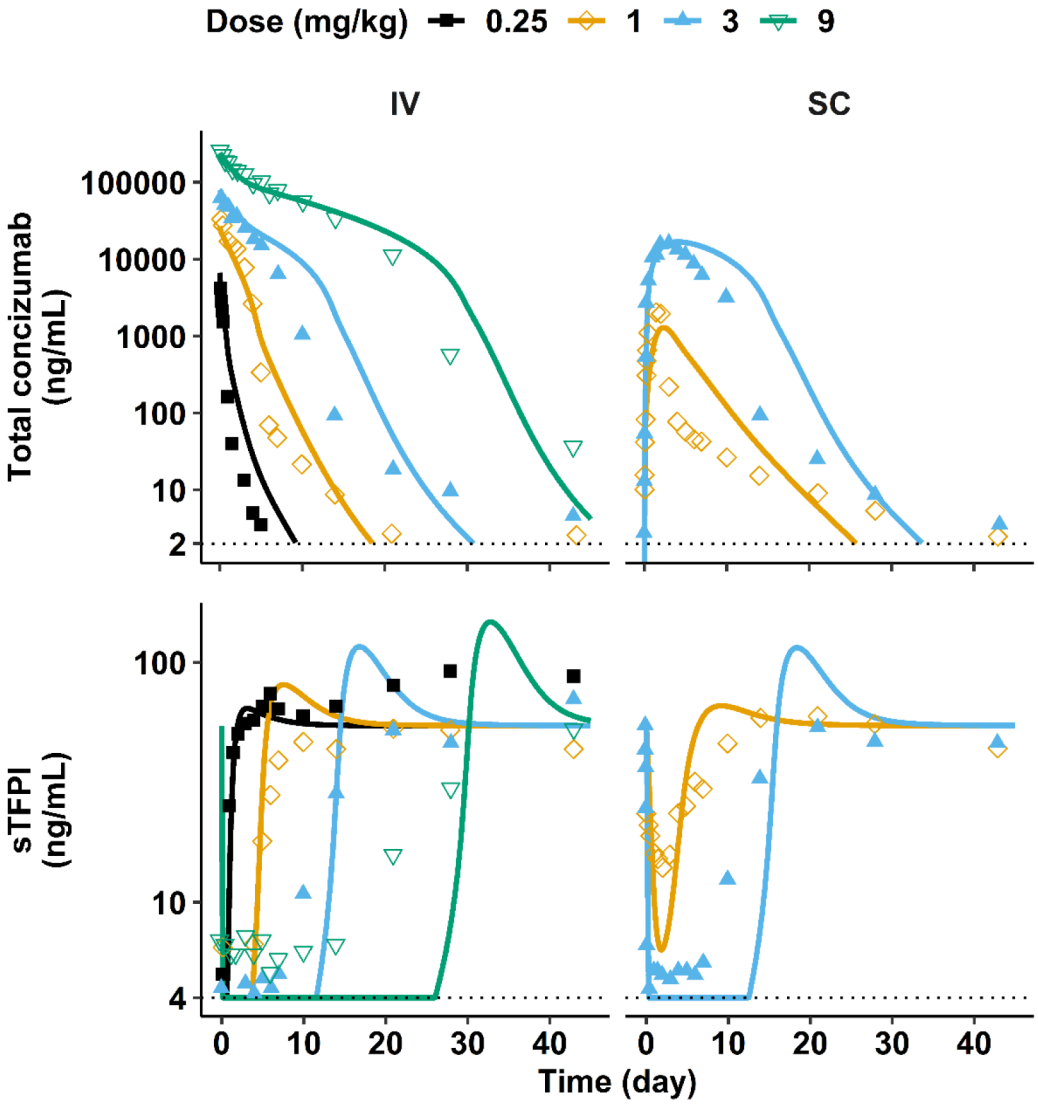

Figure 2.

The systems PK/PD model simulations of total antibody and free sTFPI in humans after IV and SC administration of concizumab. The dotted horizontal lines are the reported lower limit of quantification (LLOQ) for concizumab (Agerso et al., 2014) and sTFPI (Duckers et al., 2008).

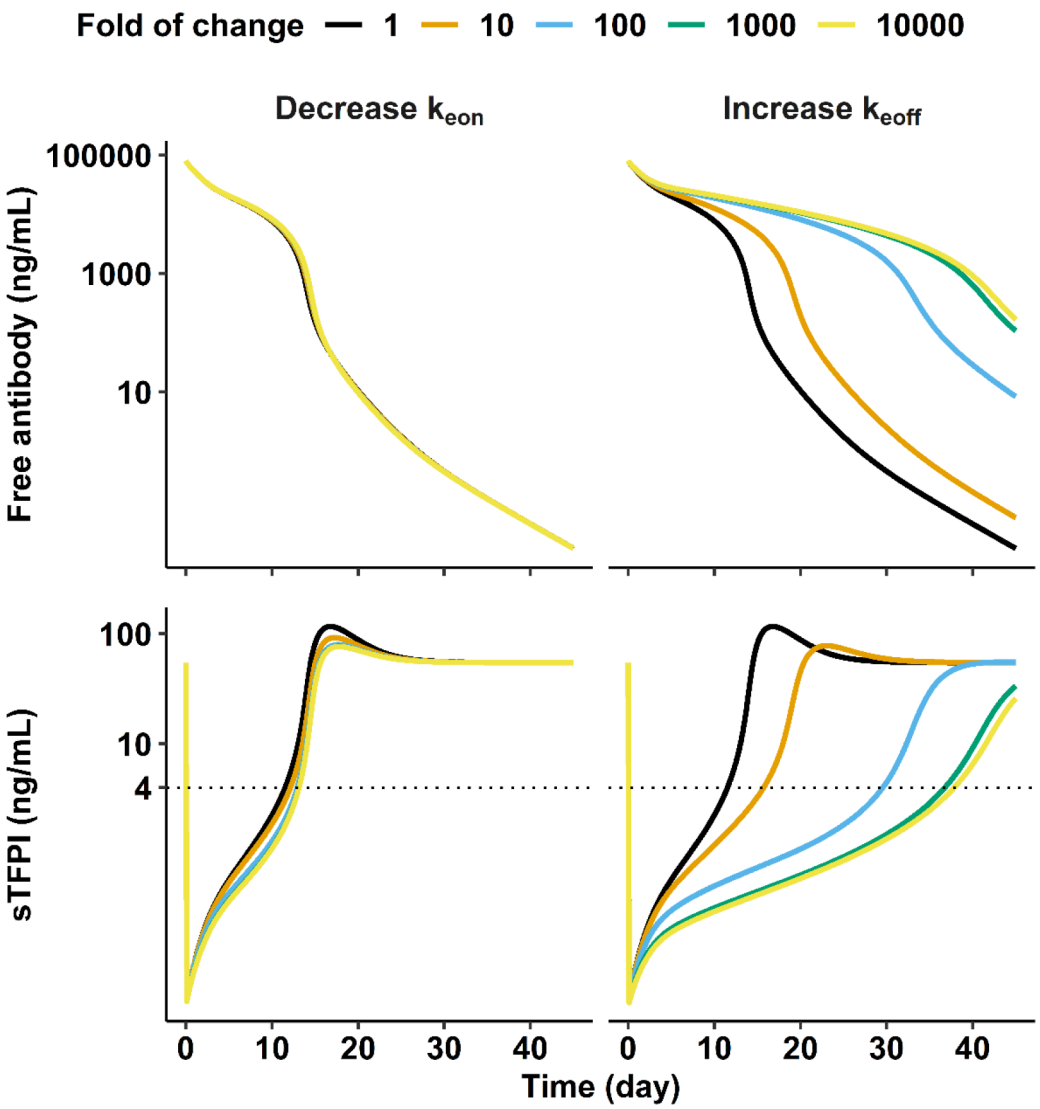

Figure 3.

The systems PK/PD model simulations of anti-TFPI recycling antibodies in humans at IV dose of 3 mg/kg. Recycling antibodies were simulated by either decreasing the antibody-mTFPI/sTFPI association rate constant (k_{eon}, left) or increasing the dissociation rate constant (k_{eoff}, right) in endosomes. The dotted horizontal lines are the LLOQ for sTFPI (Duckers et al., 2008).

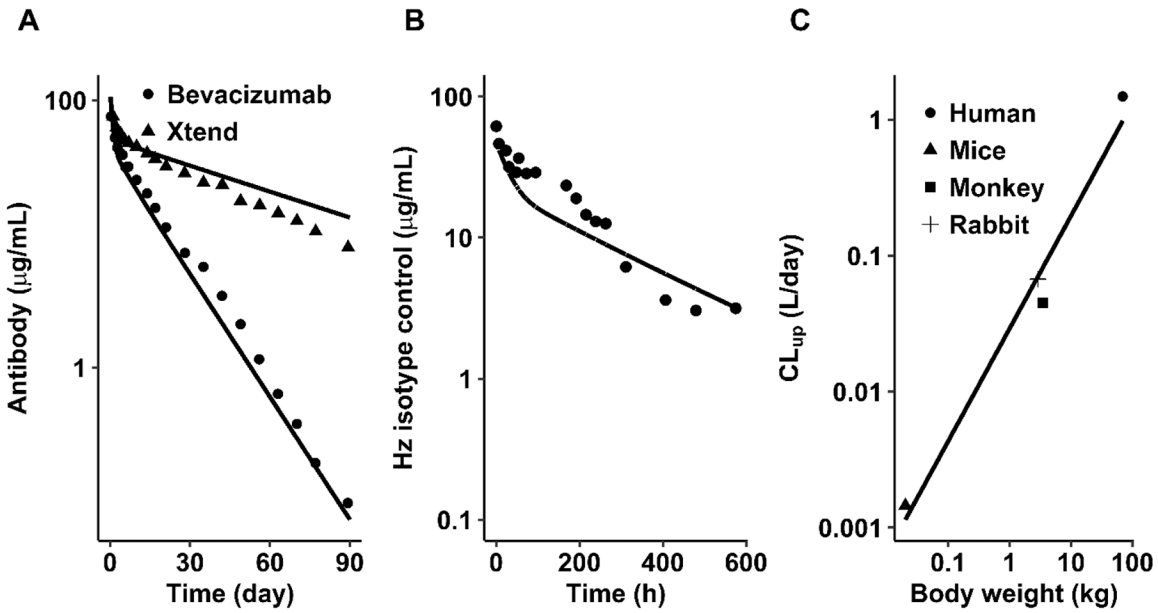

Figure 4.

Optimization of antibody nonspecific pinocytosis (CL_{up}) across species. CL_{up} was optimized using PK data of linearly cleared antibodies: **(A)** Bevacizumab and the Fc-engineered variant of bevacizumab, Xtend, in monkeys at IV 4 mg/kg; **(B)** Concizumab Hz isotype control in rabbits at IV 2 mg/kg. **(C)** Allometry of CL_{up} across species based on body weight (BW). $CL_{up} = 0.029BW^{0.83}$, $R^2 = 0.98$. Symbols are observations, lines are model predictions.

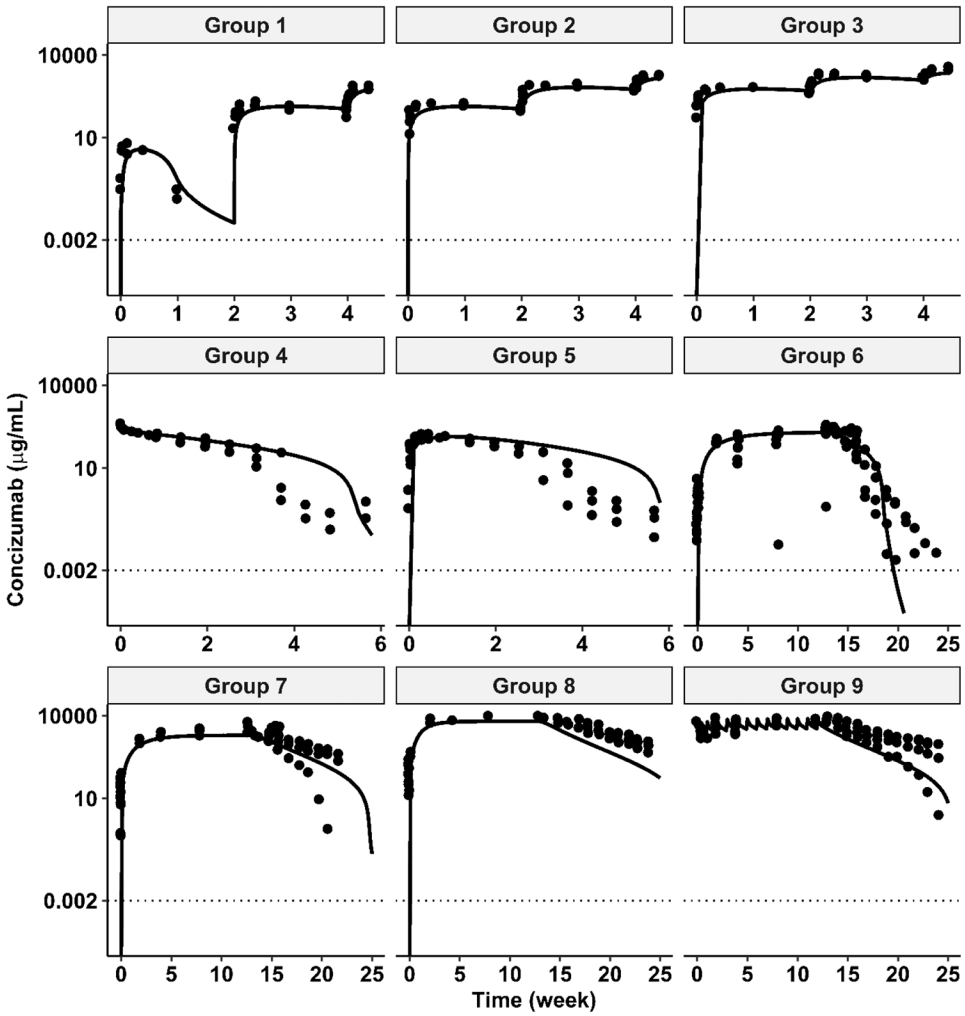

Figure 5.

The systems PK/PD model simulations of concizumab in monkeys. The symbols are observations and lines are model predictions. Dotted horizontal lines are the reported LLOQ for concizumab (Agerso et al., 2014). Group 1, 2, and 3: SC single dose escalation study at two-week intervals, 2-20-80 mg/kg, 20-80-160 mg/kg, and 80-160-200 mg/kg, respectively; Group 4 and 5: IV and SC single dose at 20 mg/kg; Group 6, 7 and 8: SC 91 daily doses at 1 mg/kg, 10 mg/kg, and 50 mg/kg, respectively; Group 9: IV 13 daily doses at 200 mg/kg.

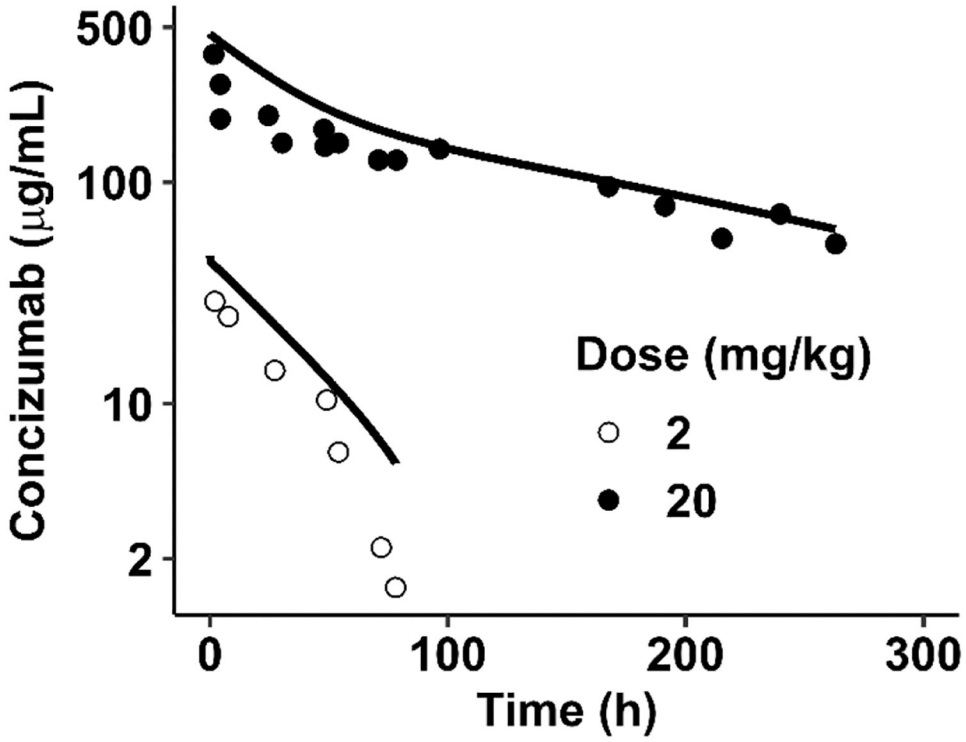

Figure 6.
The systems PK/PD model simulations of concizumab in rabbits after IV administration at 2 and 20 mg/kg. The symbols are observations and the lines are model predictions.

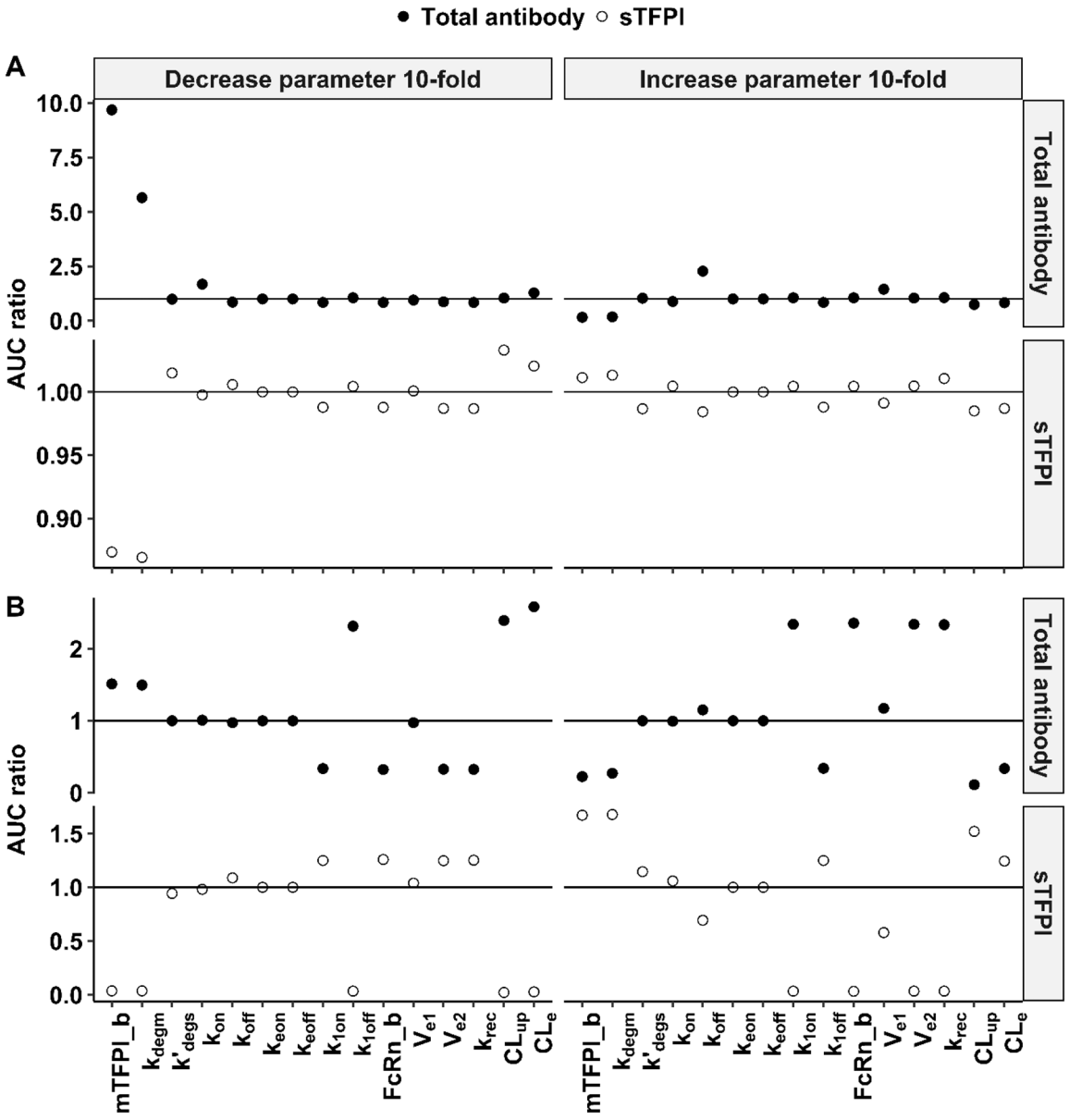

Figure 7. Local sensitivity analysis of the systems PK/PD model.

Each simulation was done by individually decreasing or increasing the parameter value 10-fold. Outputs are the AUC ratio of total antibody and free sTFPI (AUC_{after}/AUC_{before}). The simulations were done at two IV doses: **(A)** 0.25 mg/kg and **(B)** 9 mg/kg. The horizontal line indicates AUC ratio = 1.

Table 1.

Optimized parameters in the reduced PK/PD model for 70 kg humans

Parameter	Unit	Initial estimate	Model estimate	CV%
k_{on}	$M^{-1}{\cdot}s^{-1}$	4.48×10^{6} (Hilden et al., 2012)	4.48×10^{6} (Fixed)	
k_{off}	S^{-1}	1.01×10^{-4} (Hilden et al., 2012)	1.74×10^{-3}	56.12
k_{degs}	day^{-1}	1.18 (Farrokhi et al., 2018)	1.18 (Fixed)	
mTFPI_b	nM	[a] 1.6 (Hansen et al., 2014)	20.03	13.45
[b] k_{degm}, k_{int}	day^{-1}	33.12 (Mayor et al., 1998)	1.155	13.56
CL_{linear}	$L{\cdot}day^{-1}$	0.2496 (Cao and Jusko, 2014)	0.2496 (Fixed)	0.002
Additive error for total concizumab	nM	0.1	0.07952	26.76
Proportional error for total concizumab		0.1	0.3958	11.42
Additive error for free sTFPI	nM	0.1	0.1843	15.99
Proportional error for free sTFPI		0.1	0.2228	22.52

[a] The initial estimate was assumed equal to sTFPI baseline;

[b] Assume $k_{degm} = k_{int}$ to improve parameter identifiability (Gibiansky and Gibiansky, 2010).

Table 2.

Model parameter values for the systems PK/PD model in humans, monkeys, and rabbits

Parameter	Unit	Humans	Monkeys	Rabbits
Physiological parameters				
Body weight	kg	70	3.5	2.9
V_p	L	2.6 (Cao et al., 2013)	0.157 (Zhao et al., 2015)	0.107 (Armin et al., 1952)
V_{isf}	L	15.6 (Cao et al., 2013)	0.735 (Zhao et al., 2015)	0.764 (Pavlin et al., 1986)
K_p	-		0.4 (Cao et al., 2013)	
V_l	L	5.2 (Cao et al., 2013)	[a] 0.314 (Zhao et al., 2015)	[a] 0.153 (Armin et al., 1952)
L	L·day^{-1}	2.904 (Cao et al., 2013)	0.288 (Zhao et al., 2015)	0.144 (Zhao et al., 2015)
σ_1	-		0.945 (Cao et al., 2013)	
σ_2	-		0.697 (Cao et al., 2013)	
σ_l	-		0.2 (Cao et al., 2013)	
Target parameters				
k_{on}	M^{-1}·s^{-1}		4.48×10^6 (Hilden et al., 2012)	
k_{off}	s^{-1}		[b] 1.74×10^{-3}	
sTFPI_b	nM	1.6 (Hansen et al., 2014)	0.91 (Gu et al., 2017)	1.4 (Hansen et al., 2014)
k_{degs}	day^{-1}	1.18 (Farrokhi et al., 2018)	[c] 2.50	[c] 2.62
mTFPI_b	nM	[b] 20.03	[d] 11.32	[d] 17.50
k_{degm}/k_{int}	day^{-1}	[b] 1.155	[c] 2.44	[c] 2.56
Endosome parameters				
CL_{up}	L·day^{-1}	1.48 (Yuan et al., 2018)	[e] 0.045	[e] 0.0672
k_{rec}	day^{-1}		124.7 (Hopkins and Trowbridge, 1983)	
CL_e	L·day^{-1}	5.75 (Yuan et al., 2018)	[c] 0.61	[c] 0.53
V_{e1}	L		[f] 0.005% of body weight (Li et al., 2014)	
V_{e2}	L			
FcRn_b	nM		49800 (Shah and Betts, 2012)	
k_{1on}	M^{-1}·s^{-1}		[g] 2.41×10^5	
k_{1off}	s^{-1}		[g] 0.162	
SC absorption parameters				
F	-	[h] 0.93	0.93 (Agerso et al., 2014)	-
k_a	day^{-1}	[h] 0231	0.231 (Agerso et al., 2014)	-

[a] Assume equal to blood volume (Cao et al., 2013);

[b] Optimized in the reduced PK/PD model;

[c] Scaled from human value using a scaling factor of −0.25 for rate constant and 0.75 for clearance based on body weight;

[d] sTFPI and mTFPI are produced through alternative splicing of the same TFPI gene (Maroney et al., 2010). Based on the sTFPI baseline, monkeys and rabbits were calculated as $human\ mTFPI\_b \times \frac{animal\ sTFPI\_b}{human\ sTFPI\_b}$;

[e] Optimized using PK data of antibodies that show linear clearance (Figure 4);

[f] Assume the volume of endosome is 1% of cell volume and the total endothelial cell volume is 0.5% of total tissue volume (Li et al., 2014);

[g] Assume equal to the binding affinity of adalimumab, a wild-type IgG_1, to human FcRn (Suzuki et al., 2010). The IgG isotype has a negligible influence on FcRn binding (Neuber et al., 2014; Vidarsson et al., 2014). Monkey FcRn and rabbit FcRn have been shown to bind human IgG with similar affinity as human FcRn (Szikora et al., 2017; Yeung et al., 2010);

[h] Assume equal to monkey value.